Neuron
Article

In Vivo Activation of Midbrain Dopamine Neurons via Sensitized, High-Affinity α6* Nicotinic Acetylcholine Receptors

Ryan M. Drenan,[1] Sharon R. Grady,[2] Paul Whiteaker,[2,6] Tristan McClure-Begley,[2] Sheri McKinney,[1] Julie M. Miwa,[3] Sujata Bupp,[3] Nathaniel Heintz,[3] J. Michael McIntosh,[4] Merouane Bencherif,[5] Michael J. Marks,[2] and Henry A. Lester[1,*]
[1]Division of Biology, California Institute of Technology, Pasadena, CA 91125, USA
[2]Institute for Behavioral Genetics, University of Colorado Boulder, Boulder, CO 80309, USA
[3]The Laboratory of Molecular Biology, Howard Hughes Medical Institute, Rockefeller University, New York, NY 10021, USA
[4]Departments of Psychiatry and Biology, University of Utah, Salt Lake City, UT 84112, USA
[5]Department of Preclinical Research, Targacept Inc., Winston-Salem, NC 27101, USA
[6]Present address: Barrow Neurological Institute, St. Joseph's Hospital and Medical Center, Phoenix, AZ 85013, USA
*Correspondence: lester@caltech.edu
DOI 10.1016/j.neuron.2008.09.009

SUMMARY

α6-containing (α6*) nicotinic ACh receptors (nAChRs) are selectively expressed in dopamine (DA) neurons and participate in cholinergic transmission. We generated and studied mice with gain-of-function α6* nAChRs, which isolate and amplify cholinergic control of DA transmission. In contrast to gene knockouts or pharmacological blockers, which show necessity, we show that activating α6* nAChRs and DA neurons is sufficient to cause locomotor hyperactivity. $\alpha6^{L9'S}$ mice are hyperactive in their home cage and fail to habituate to a novel environment. Selective activation of α6* nAChRs with low doses of nicotine, by stimulating DA but not GABA neurons, exaggerates these phenotypes and produces a hyperdopaminergic state in vivo. Experiments with additional nicotinic drugs show that altering agonist efficacy at α6* provides fine tuning of DA release and locomotor responses. α6*-specific agonists or antagonists may, by targeting endogenous cholinergic mechanisms in midbrain or striatum, provide a method for manipulating DA transmission in neural disorders.

INTRODUCTION

Identification of the relevant nAChRs involved in (1) normal DA transmission, (2) disorders of the DA system, such as schizophrenia, Parkinson's disease, and ADHD, and (3) nicotine dependence is a major priority. α6* (* indicates that other subunits may be present in the pentameric receptor) nAChRs are highly and selectively expressed in DA neurons, with additional functional expression in locus coeruleus and retinal ganglion cells (Azam and McIntosh, 2006; Azam et al., 2002; Champtiaux et al., 2002; Gotti et al., 2005b; Le Novere et al., 1996). α6* nAChRs are selectively inhibited by the marine cone snail peptide α-conotoxin MII (αCtxMII) (Cartier et al., 1996; Whiteaker et al., 2000). Immunoprecipitation and αCtxMII-binding studies demonstrated that α6β2β3* and α6α4β2β3* pentamers are the predominant α6* nAChRs in striatum (Champtiaux et al., 2003; Zoli et al., 2002). α6β2* receptors account for ~30% of nicotine-stimulated DA release in striatum (Grady et al., 2002; Kaiser et al., 1998; Kulak et al., 1997). β3 subunits are encoded by a gene adjacent to *Chrna6*, are usually coexpressed with α6, and are essential for α6* nAChR biogenesis and function (Cui et al., 2003; Gotti et al., 2005a). α6* receptors exhibit the highest known sensitivity to nicotine and ACh in functional measurements on native receptors (Salminen et al., 2004) yet function poorly in heterologous expression systems (Drenan et al., 2008). As a result, there has been little progress in defining selective agonists for α6* nAChRs or on other functional measurements. Furthermore, in midbrain DA neurons, studies of somatodendritic α6* receptors are complicated by the presence of α4β2* (non-α6), and selective antagonists of α4β2* (non-α6) have not been identified.

Many experiments with selective destruction of DA neurons show that the activity of such neurons is necessary for reinforcement of natural and artificial rewards. These cells exhibit tonic and phasic firing patterns (Grenhoff et al., 1986), where phasic or "burst" firing carries salient information thought to predict imminent reward status (Schultz, 2002). Pedunculopontine tegmentum (PPTg) and laterodorsal tegmentum (LDTg) fibers provide a cholinergic drive that strongly regulates DA neuron excitability and the transition to burst firing (Lanca et al., 2000). Midbrain nAChRs in three locations respond to mesopontine-derived ACh: (1) α7* nAChRs on glutamatergic terminals from cerebral cortex, (2) α4β2* nAChRs on GABAergic terminals and cell bodies, and (3) α4* and α6* somatodendritic nAChRs on DA neurons (Calabresi et al., 1989). Nicotine interferes with normal cholinergic transmission to DA neurons, in part by modifying the weights of these various nAChR synapses. For example, nicotine at concentrations found in the CSF of smokers preferentially desensitizes α4β2* nAChRs regulating midbrain GABA release (Mansvelder et al., 2002) yet still permits α7* nAChR-regulated glutamate release (Mansvelder and McGehee, 2000). This produces both disinhibition and direct excitation of DA neurons, increasing the probability of a switch to burst firing.

Nicotine also exaggerates the action of endogenous ACh in regulating DA release in striatum. Striatal cholinergic interneurons continually release ACh that activates nAChRs, which maintains background DA levels during tonic firing of midbrain DA neurons (Zhou et al., 2001). However, DA release in response to burst firing of DA neurons is facilitated by a reduction in nAChR activity (Rice and Cragg, 2004; Zhang and Sulzer, 2004). α6* receptors, due to their high sensitivity and their selective expression in DA cell bodies and presynaptic terminals, are probably key players in cholinergic control of DA release. We reasoned that genetic "sensitization" of these receptors would (1) amplify the role of α6* nAChRs in cholinergic control of DA transmission and (2) allow for selective pharmacological stimulation of these neurons. This approach would complement previous experiments using α6 knockout mice and α6* pharmacological blockade, demonstrating behavioral and physiological responses for which α6* nAChRs are sufficient.

We introduced a bacterial artificial chromosome (BAC) transgene into the mouse germline with a mutant copy of the mouse *Chrna6* gene that rendered mutant α6* channels "hypersensitive" to endogenous ACh or exogenous nicotine. DA neuron excitability and DA release is greatly augmented in these mice, and they exhibit behavioral phenotypes consistent with increased DA neuron firing and/or DA release. These studies improve our knowledge of cholinergic regulation of the midbrain DA system and of α6* nAChR biology and have implications for the treatment of disorders involving changes in DA.

RESULTS

Production and Characterization of BAC $\alpha6^{L9'S}$ Transgenic Mice

We selected a 156 kb mouse BAC clone containing the genomic *Chrna6* (α6 nAChR) locus with substantial 5′ and 3′ flanking genomic regions for generating a targeting construct to faithfully recapitulate expression of *Chrna6*. α6 Leu280 (the Leu 9′ residue in the M2 domain) was mutated to Ser via homologous recombination using a two-step selection/counterselection procedure in *E. coli*. (Figure S1A available online). The final construct was injected into fertilized mouse eggs, and six transgenic offspring were identified by genomic DNA sequencing and diagnostic PCR (Figure S1B and S1C). To eliminate possible artifacts of transgene position/insertion, we analyzed two independently derived lines (lines 2 and 5), which have different transgene copy numbers (Figure S1D) and different genomic positions. Both mouse lines expressed mutant $\alpha6^{L9'S}$ mRNA in addition to wild-type (WT) α6 mRNA (Figure S1E).

We found no difference in location or intensity of [^{125}I]-α-conotoxin MII (αCtxMII) labeling in $\alpha6^{L9'S}$ versus WT brains, confirming correct regional expression of α6* nAChRs in mutant mice (Figure S1F). To corroborate this, we quantified α6*-binding sites. Membranes were prepared from striatum (ST), olfactory tubercle (OT), superior colliculus (SC) (regions that account for most α6*-binding sites), and thalamus (TH) (where most binding sites are α4β2*). [^{125}I]-epibatidine binding, coupled with inhibition by unlabeled αCtxMII, revealed α6* and non-α6* (α4β2*) receptors (Figure S1G). Collectively, these results indicate that $\alpha6^{L9'S}$ mice exhibit normal levels and localization of neuronal nAChRs.

Spontaneous and Nicotine-Induced Hyperactivity in $\alpha6^{L9'S}$ Mice

We measured home cage horizontal locomotor activity for WT and $\alpha6^{L9'S}$ mice over a period of 48 hr. $\alpha6^{L9'S}$ mice were markedly hyperactive relative to WT control littermates (Figure 1A). This effect was restricted to lights off (Figure 1B), though there was a nonsignificant trend toward hyperactivity during lights on. Although WT mice show locomotor habituation when placed into a novel environment, $\alpha6^{L9'S}$ mice exhibit sustained activity. We measured WT and $\alpha6^{L9'S}$ locomotor activity for 30 min after placement in a new home cage environment (Figure 1C). Activity during the first 15 min of the session was unchanged, but from t = 16 to 30 min, $\alpha6^{L9'S}$ mice exhibited significantly greater activity than WT littermates (Figure 1D).

α6* nAChRs are highly expressed in DAergic neurons, and nicotine has psychomotor stimulant properties in rodents. We injected WT and $\alpha6^{L9'S}$ mice with nicotine and measured locomotor activity. Low doses of nicotine (0.15 mg/kg, i.p.) strongly activated locomotion in $\alpha6^{L9'S}$ mice but had no effect in WT mice (Figure 1E). To characterize the locomotor activation phenotype in $\alpha6^{L9'S}$ mice, we constructed a nicotine dose-response relation. WT mice exhibited locomotor suppression at doses of nicotine between 0.5 and 2.0 mg/kg, i.p. (Figure 1F), consistent with previous work (Tapper et al., 2007). In contrast, $\alpha6^{L9'S}$ mice exhibited steadily increasing locomotor responses between 0.02 and 0.15 mg/kg, i.p. nicotine, followed by a decline at 0.4 mg/kg, i.p and locomotor suppression similar to WT mice at 1.5 mg/kg, i.p. Thus, selective activation of α6* receptors results in locomotor activation rather than locomotor suppression. This phenotype was not a stress response, as saline injections did not produce locomotor activation (Figure 1G).

Locomotor activation in $\alpha6^{L9'S}$ mice was dependent on activation of nicotinic receptors; we noted a strong block of the locomotor response in $\alpha6^{L9'S}$ (but not WT) mice preinjected with mecamylamine (1 mg/kg, i.p.) (Figure 1H). Further, $\alpha6^{L9'S}$ locomotor activation acted through dopamine receptors; the response to 0.15 mg/kg, i.p. nicotine was completely inhibited by SCH23390 (D1DR antagonist; 2 mg/kg, i.p.) and partially inhibited by sulpiride (D2DR antagonist; 20 mg/kg, i.p.) (Figure 1H).

To determine whether $\alpha6^{L9'S}$ mice develop tolerance or sensitization to nicotine psychomotor stimulation, we injected groups of $\alpha6^{L9'S}$ mice once daily for 6 days with nicotine. Injection of 0.02 mg/kg, i.p. or 0.08 mg/kg, i.p. nicotine did not produce any change in locomotor behavior after repeated injections (Figure 1I). Nicotine also produces hypothermia in mice, and α4* hypersensitive mice exhibit this effect at nicotine doses ~50-fold lower than WT mice (Tapper et al., 2004). We found no difference between the hypothermia responses of WT and $\alpha6^{L9'S}$ mice (data not shown).

Augmented Nicotine-Stimulated DA Release from Presynaptic Terminals in $\alpha6^{L9'S}$ Mice

Mouse α6* nAChRs expressed in midbrain DA neurons are located both on the cell body and on presynaptic terminals in caudate/putamen (CPu), nucleus accumbens (NAc), and striatal aspects of the olfactory tubercle (OT). We measured nicotine-stimulated [^{3}H]DA release from striatal synaptosomes of WT and $\alpha6^{L9'S}$ mice. We made separate tissue samples containing

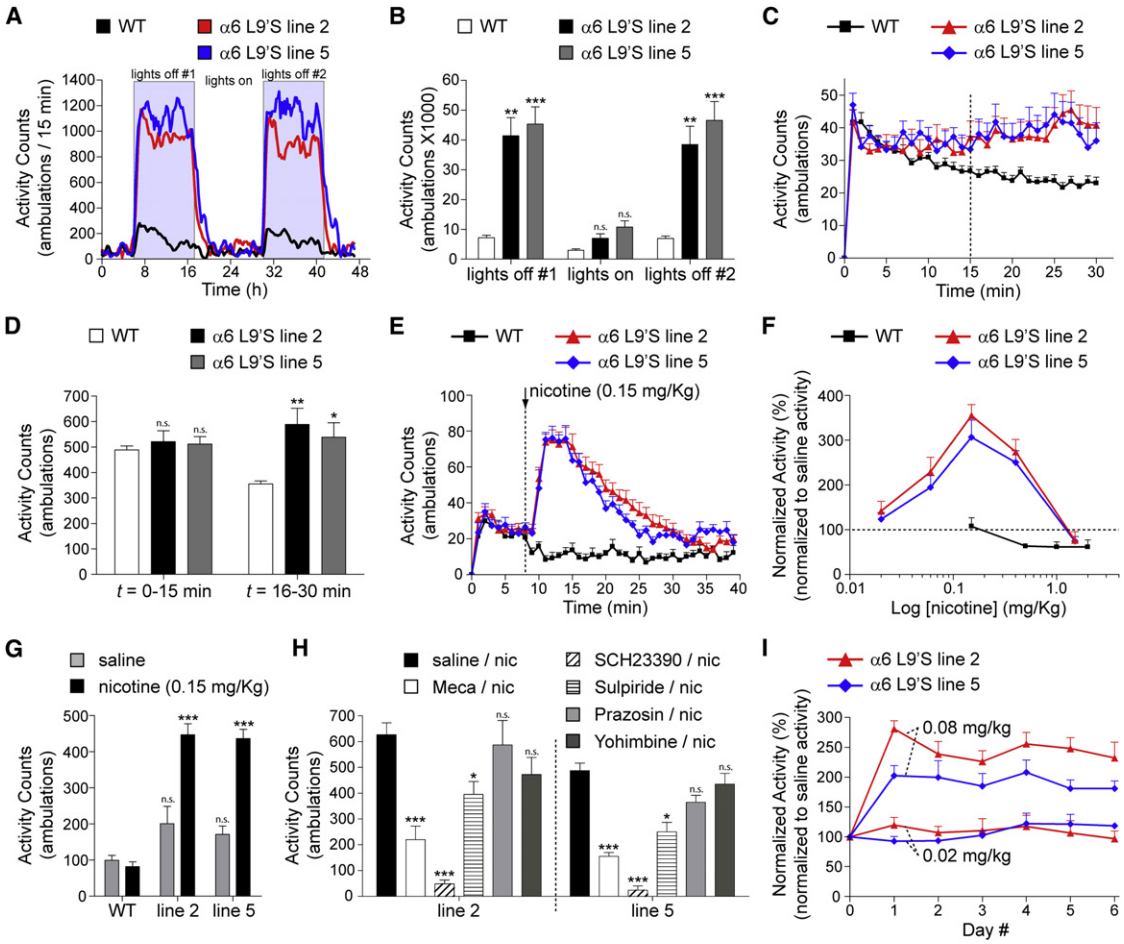

Figure 1. $\alpha6^{L9'S}$ Mice Are Markedly Hyperactive and Hypersensitive to the Psychomotor Stimulant Action of Nicotine

(A and B) $\alpha6^{L9'S}$ mice are hyperactive in their home cage. Horizontal locomotor activity of mice ($\alpha6^{L9'S}$ or WT cagemates) in their home cage environment was recorded during a 48 hr period. Raw locomotor activity data (number of ambulations/15 min period) are reported (A). Total locomotor activity from "lights on" and "lights off" periods indicated in (A) are shown (B) for WT and $\alpha6^{L9'S}$ mice.

(C and D) $\alpha6^{L9'S}$ mice do not habituate to a novel environment. Mice ($\alpha6^{L9'S}$ or WT cagemates) were removed from their home cage and immediately placed in a fresh cage. Locomotor activity was measured for 30 min. Raw locomotor activity data (number of ambulations/min) are reported (C). Total locomotor activity from (C) for t = 0–15 min or t = 16–30 min is shown (D).

(E) Nicotine specifically stimulates locomotor activity in $\alpha6^{L9'S}$ transgenic mice. After 8 min of baseline locomotor activity, mice (WT, $\alpha6^{L9'S}$ line 2 and 5) were injected with 0.15 mg/kg i.p. nicotine. Locomotor activity was recorded for an additional 30 min after injection. Raw locomotor activity data (number of ambulations/min) are reported.

(F) Dose-response relationship for nicotine-stimulated locomotor activity in WT and $\alpha6^{L9'S}$ mice. Mice were administered nicotine at the indicated dose, and total locomotor activity was measured as in (E). Locomotor activity for each mouse was normalized to a saline control injection for the same mouse. Data are expressed as the percentage of the response to saline (set to 100%).

(G) Locomotor activity following saline or nicotine (0.15 mg/kg, i.p.) injection in WT and $\alpha6^{L9'S}$ mice. Total raw locomotor activity data (number of ambulations/min, 30 min total) are reported.

(H) Behavioral pharmacology of nicotine-stimulated locomotor activation in $\alpha6^{L9'S}$ mice. Mice (WT or $\alpha6^{L9'S}$) were preinjected with saline, mecamylamine (1 mg/kg, i.p.), SCH23390 (2 mg/kg, i.p.), sulpiride (20 mg/kg, i.p.), prazosin (1 mg/kg, i.p.), or yohimbine (1 mg/kg, i.p.) immediately prior to the start of data acquisition. Nicotine (0.15 mg/kg, i.p.) was injected a t = 8 min, and locomotor activity was measured for an additional 30 min. Total raw locomotor activity data (number of ambulations/min, 30 min total) are reported.

(I) Lack of sensitization or tolerance following repeated nicotine administration in $\alpha6^{L9'S}$ mice. Groups of $\alpha6^{L9'S}$ mice were injected with saline once daily for 3 consecutive days, followed by nicotine (0.02 mg/kg, i.p., or 0.08 mg/kg, i.p.) once daily for 6 consecutive days. Locomotor activity was measured as in (E), and nicotine-stimulated locomotor activity for each mouse was normalized to saline control injections (average of three saline injections) for the same mouse. Data are expressed as the percentage of the response to saline (set to 100%).

All data are expressed as mean ± SEM. *p < 0.05, **p < 0.01, ***p < 0.001.

striatum (ST; CPu and dorsal aspects of NAc) and olfactory tubercle (OT). Because CPu receives DAergic projections mainly from substantia nigra whereas OT receives DAergic projections exclusively from VTA, this preparation crudely separates the mesostriatal and mesolimbic pathways. For total DA release in ST, there was no difference in R_{max} (Figures 2A and S2) and

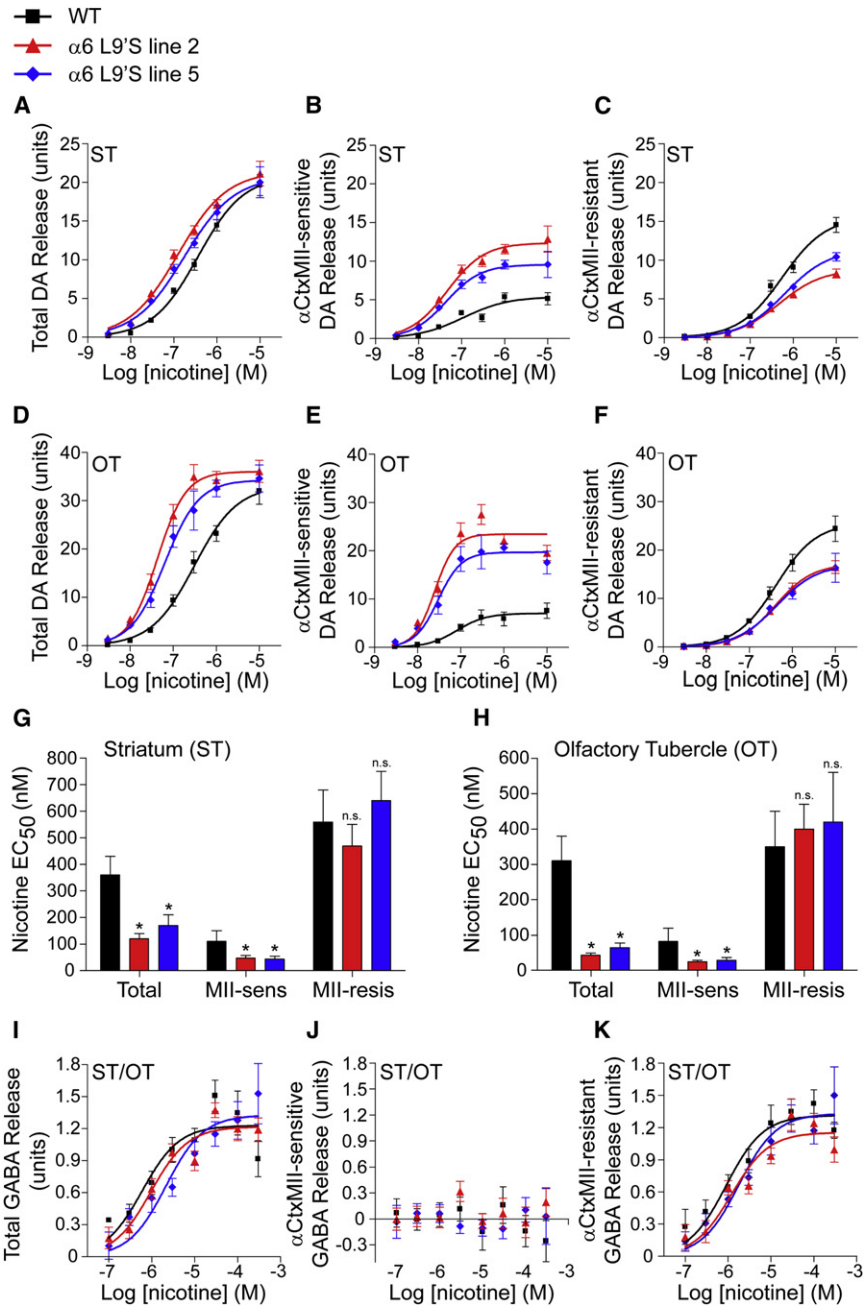

Figure 2. Presynaptic α6* nAChRs in Striatum Mediate Hypersensitive, Nicotine-Stimulated DA Release in $\alpha6^{L9'S}$ Transgenic Mice

(A–C) Hypersensitive DA release in striatum of $\alpha6^{L9'S}$ transgenic mice is α6* dependent. Striata ("ST"; dorsal striatum and dorsal aspects of nucleus accumbens) from WT and $\alpha6^{L9'S}$ mice were dissected and synaptosomes were prepared. DA release was stimulated with a range of nicotine concentrations (3 nM, 10 nM, 30 nM, 100 nM, 300 nM, 1 μM, 10 μM), and a concentration-response relation for each mouse line (n = 6 mice/line) is shown for total release (A). To determine the relative contribution of α6* and non-α6* receptors, striatal synaptosome samples were incubated with αCtxMII (50 nM). α6*-independent release is shown in (C), and αCtxMII-sensitive (α6* dependent) release is shown in (B).

(D–F) Hypersensitive DA release in olfactory tubercle of $\alpha6^{L9'S}$ transgenic mice is α6* dependent. Olfactory tubercle ("OT") was dissected from WT and $\alpha6^{L9'S}$ mice, and samples were processed as in (A)–(C).

(G and H) Quantification of hypersensitive DA release in striatum (G) and olfactory tubercle (H). Average nicotine EC_{50} values for each concentration-response curve from (A)–(F) are shown.

(I–K) α6* nAChRs do not participate in nicotine-stimulated GABA release in striatum. ST and OT were dissected and combined, followed by synaptosome preparation. GABA release was stimulated by nicotine at the following concentrations: 100 nM, 300 nM, 1 μM, 3 μM, 10 μM, 30 μM, 100 μM, and 300 μM. Total (I) release and αCtxMII-sensitive (J) and resistant (K) components are shown.

Data are expressed as mean ± SEM. *$p < 0.05$.

a small but significant reduction in EC_{50} for both transgenic lines relative to WT (Figure 2G). In OT, there was a slight increase in R_{max} (Figures 2D and S2) and a greater reduction in the EC_{50} for $\alpha6^{L9'S}$ lines compared to WT (Figure 2H). We used αCtxMII to inhibit α6* receptors, revealing the contribution of α6* and non-α6* nAChRs to this augmented DA release. In ST and OT, we observed a significant increase in total DA release mediated by α6 at most nicotine concentrations (Figures 2B and 2E). Interestingly, this was accompanied by a concomitant decrease in the non-α6* (α4β2* mediated) component (Figures 2C and 2F) in $\alpha6^{L9'S}$ samples. In ST and OT, we measured a significant reduction in the EC_{50} for the α6-dependent component and no change in EC_{50} for the non-α6 component (Figures 2G and 2H). Overall, DA release from $\alpha6^{L9'S}$ striatal synaptosomes may be underestimated by this assay, as 20 mM K^+ stimulated slightly less DA release in both $\alpha6^{L9'S}$ lines relative to WT mice (Figure S2). These results directly reveal that selective α6* activation is capable of stimulating striatal DA release.

α4β2* nAChRs modulate striatal GABA release (Lu et al., 1998). We measured GABA release from striatal (ST and OT combined) synaptosomes of WT and $\alpha6^{L9'S}$ mice to determine whether any α6*-dependent component was revealed by the gain-of-function L9′S mutation. There was no difference in total GABA release for any genotype comparison (Figures 2I and S3), and there was no α6* component (Figures 2J, 2K, and S3). A Student's t test on R_{max} and EC_{50} values revealed no significant difference between total and αCtxMII-resistant GABA release for any genotype (WT R_{max} p = 0.47, WT EC_{50} p = 0.73; line 2 R_{max} p = 0.93, line 2 EC_{50} p = 0.31; line 5 R_{max} p = 0.62, line 5 EC_{50} p = 0.63). Furthermore, there was no significant difference between any genotype on R_{max} or EC_{50} (two-way ANOVA with Tukey post

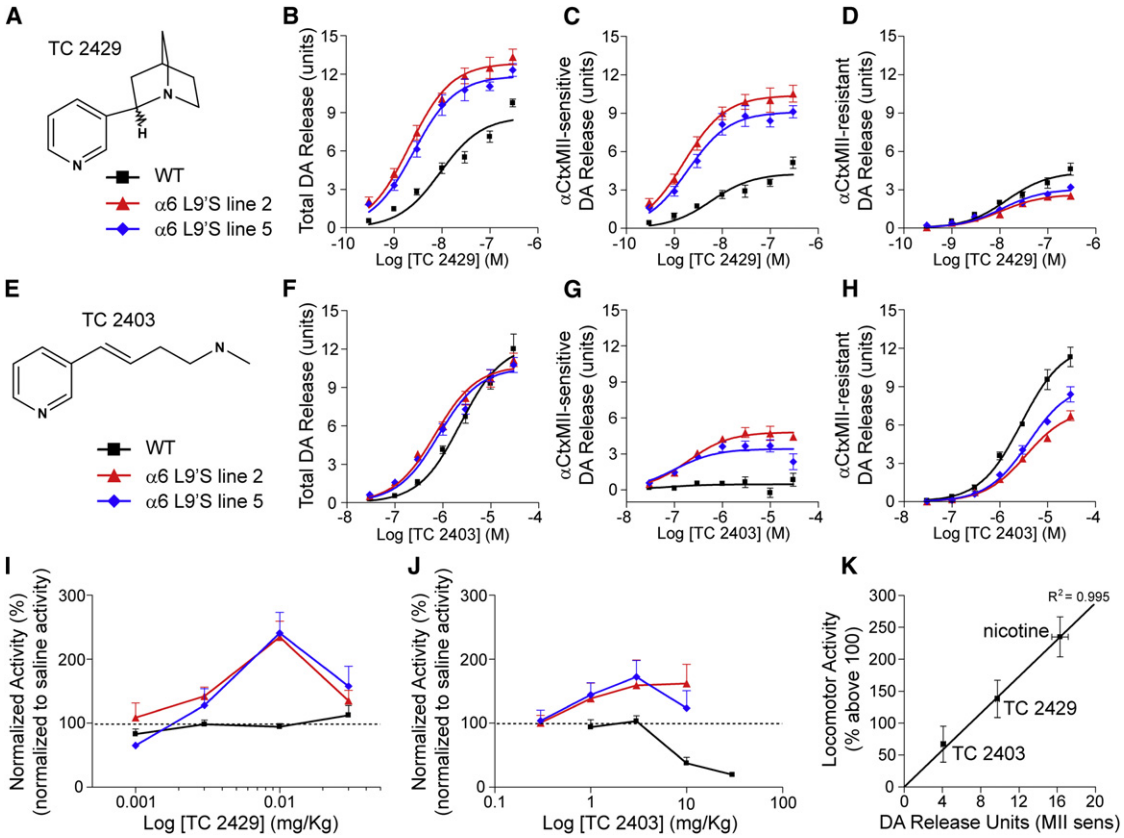

Figure 3. α6-Dependent Neurotransmitter Release and Behavioral Phenotypes Are Discriminated by Subtype-Selective Nicotinic Compounds

(A) TC 2429 structure.

(B–D) An α6*-selective nicotinic agonist demonstrates enhanced striatal DA release in $\alpha6^{L9'S}$ mice. Striatum (ST) and olfactory tubercle (OT) from WT and $\alpha6^{L9'S}$ mice were dissected and combined, followed by synaptosome preparation. DA release was stimulated with a range of nicotine concentrations (see Figure 2A), and total (B) release as well as αCtxMII-sensitive (C) and αCtxMII-resistant (D) components are shown for each genotype.

(E) TC 2403 structure.

(F–H) An α4*-selective nicotinic agonist modestly activates striatal α6* nAChRs in $\alpha6^{L9'S}$ mice. Similar to (B)–(D), total DA release (F) as well as αCtxMII-sensitive (G) and αCtxMII-resistant (H) components are shown for TC 2403.

(I) An α6*-selective agonist stimulates locomotor activity in $\alpha6^{L9'S}$ mice without affecting WT activity. Mice were administered TC 2429 at the indicated dose, and total locomotor activity was measured as in Figure 1. Locomotor activity for each mouse was normalized to saline control injections in the same mouse.

(J) α6* nAChR stimulation by TC 2403 induces modest locomotor activity in $\alpha6^{L9'S}$ mice. Mice were administered TC 2403 at the indicated dose, and total locomotor activity was measured as in Figure 1. Locomotor activity for each mouse was normalized to saline control injections in the same mouse.

(K) Close correlation between α6*-mediated DA release and locomotor activity. For nicotine (Figure 2), TC 2429, and TC 2403, αCtxMII-sensitive DA release average R_{max} values for lines 2 and 5 (ST and OT combined) were plotted versus peak locomotor activity (percentage above 100). A regression line (R^2 = 0.995) for the three compounds is shown.

Data are reported as mean ± SEM.

hoc comparison: R_{max} $F_{(2,66)}$ = 1.87, p = 0.163; EC_{50} $F_{(2,66)}$ = 0.744, p = 0.48) nor was there any effect of αCtxMII across all genotypes on R_{max} or EC_{50} (R_{max} $F_{(1,66)}$ = 0.35, p = 0.554; EC_{50} $F_{(1,66)}$ = 0.643, p = 0.426). Stimulation with 20 mM K^+ showed no differences between WT and $\alpha6^{L9'S}$ samples for GABA release (Figure S3). This indicates that GABAergic terminals in striatum, either derived locally or from VTA or SNr GABAergic neurons, contain no appreciable α6* nAChRs.

α6* receptors synthesized in retinal ganglion cells reside in the superficial layers of superior colliculus (SC) (Gotti et al., 2005b), and we measured nicotine-stimulated $^{86}Rb^+$ efflux from SC synaptosomes. $\alpha6^{L9'S}$ SC αCtxMII-sensitive receptors are hypersensitive to nicotine relative to WT, whereas αCtxMII-resistant $^{86}Rb^+$ efflux is unchanged (Figure S4).

DA Release and Locomotor Activity Are Precisely Controlled by Varying α6* Agonist Efficacy

The DA release data suggest a mechanism involving dopamine for the psychomotor stimulant action of nicotine as well as the spontaneous hyperactivity observed. For DA release in WT mice, TC 2429 (Figure 3A) (Bhatti et al., 2008) is a full agonist (versus nicotine) with 3-fold selectivity at α6β2* and a weak partial agonist at α4β2, whereas TC 2403 (Figure 3E) (Bencherif et al., 1996; Lippiello et al., 1996) is a full agonist (versus nicotine) at

α4β2 and has no activity at α6β2* (Figure S5). TC 2429, like nicotine, was more efficacious and more potent for DA release from striatal synaptosomes of $\alpha6^{L9'S}$ mice relative to WT (Figure 3B). In both $\alpha6^{L9'S}$ lines, R_{max} was greater, and the EC_{50} was reduced relative to WT. This was entirely attributable to α6* nAChRs (Figure 3C), which accounted for a greater proportion of the total response. There was a concomitant decline in the total response but not the EC_{50} for α4β2* (αCtxMII resistant) nAChRs (Figure 3D). We characterized the ability of TC 2429 to induce psychomotor activation in $\alpha6^{L9'S}$ and WT control mice. Similar to nicotine, injections of TC 2429 stimulated locomotor activity in $\alpha6^{L9'S}$ mice but not WT (Figure 3I). Unlike nicotine, TC 2429 did not produce locomotor suppression in WT mice.

TC 2403 was slightly more potent and had equivalent efficacy for DA release in $\alpha6^{L9'S}$ versus WT striatum (Figure 3F). The increased potency was due to the amplification of an αCtxMII-sensitive response not visible in WT tissue preparations (Figure 3G). TC 2403 was a partial agonist at this receptor (Figure S5). Consistent with competition between α6 and α4 subunits for common β2 subunits, there was a decline in R_{max} in $\alpha6^{L9'S}$ mice for α4β2* (αCtxMII resistant) nAChRs (Figures 3H and S5). In locomotor assays, TC 2403 induced a slight locomotor activation in $\alpha6^{L9'S}$ but not WT mice (Figure 3J), consistent with partial activity at α6* nAChRs. Nicotine (10 μM) was used as a positive control for DA release for TC 2429 and TC 2403 (Figure S5). For nicotine, TC 2429, and TC 2403, we noted a tight correlation between α6*-dependent DA release in vitro and peak locomotor activity in vivo (Figure 3K). These results suggest a mechanism whereby agonism at α6* nAChRs stimulates striatal DA release and produces locomotor stimulation, perhaps without GABAergic attenuation, which is normally coactivated by α4β2* activation (Figures 2I–2K).

$\alpha6^{L9'S}$ Receptors Sensitize DA Neurons to Activation by Nicotine

To directly determine whether DA neurons in $\alpha6^{L9'S}$ mice express hypersensitive α6* nAChRs, we prepared coronal midbrain slices (Figure 4A) and made patch-clamp recordings from VTA DA neurons in whole-cell configuration. DA neurons can be identified based on expression of tyrosine hydroxylase (TH) (Figure 4B) and with electrophysiology (Wooltorton et al., 2003); DA neurons exhibit pacemaker firing (1–5 Hz), membrane potential adaptations in response to hyperpolarizing current injections, and often express I_h. We recorded currents induced by local nicotine application (Figure 4C) at a range of concentrations. Nicotinic currents in $\alpha6^{L9'S}$ neurons were markedly hypersensitive to nicotine; puffs of nicotine (1 μM) elicited inward currents that were larger than those seen in WT neurons at any concentration (Figure 4D). At all nicotine concentrations, $\alpha6^{L9'S}$ neurons of both transgenic lines showed larger average peak current responses than WT neurons (Figure 4E). Normalizing the peak current amplitude to cell capacitance yielded identical results (Figure S6).

Whole-cell responses to 1 μM nicotine were ≥90% blocked when αCtxMII (100 nM) was added to the perfusate (Figure 4F, upper panel). αCtxMII block persisted 30 min after washout, consistent with previous work (McIntosh et al., 2004). Likewise, responses to 1 μM nicotine were 100% blocked in the presence of dihydro-β-erythroidine (DHβE, 2 μM), a potent inhibitor of most β2* receptors (Figure 4F, lower panel). Although the general kinetics of these hypersensitive responses suggests that $\alpha6^{L9'S}$ receptors are postsynaptic, a presynaptic mechanism is not excluded by the data. To address this, we inhibited AMPA/kainate receptors with 6-cyano-7-nitroquinoxaline-2,3-dione (CNQX, 15 μM) and voltage-gated Na^+ channels with tetrodotoxin (TTX, 0.5 μM). Inward current responses to 1 μM nicotine were unaffected by either CNQX or TTX (Figure 4G). Furthermore, we found no effect (n = 6, 0% block) on peak current amplitude (1 μM nicotine) in the presence of methyllycaconitine (MLA, 10 nM) (Figure 4G). Thus, hypersensitive α6* responses were consistent with a postsynaptic mechanism.

VTA DA neuron pacemaker firing was unaltered in WT versus $\alpha6^{L9'S}$ slices (Figure 4I). To determine whether hypersensitive nicotinic receptors in $\alpha6^{L9'S}$ neurons were capable of acutely altering the excitability of VTA DA neurons, we recorded action potential firing in response to local nicotine application. Nicotine (1 μM) induced a transient increase in the instantaneous firing rate and a depolarization of the membrane potential (Figure 4H). There was a significant increase in the firing rate for $\alpha6^{L9'S}$ but not WT cells (Figure 4I).

We noticed greater fluctuations in the holding current in $\alpha6^{L9'S}$ VTA DA neurons than in WT (Figure 5A). This suggests that some $\alpha6^{L9'S}$ channels are tonically active, reminiscent of previous observations in α4 nAChR L9′S and L9′A knockin mice (Labarca et al., 2001; Shao et al., 2008). To determine whether this change in resting membrane conductance was due to active $\alpha6^{L9'S}$ channels, α6* receptors were blocked by application of αCtxMII. α6 blockade completely eliminated this increased channel noise in all $\alpha6^{L9'S}$ cells tested (Figure 5B). WT neurons bathed in αCtxMII served as a control (Figure 5C). To quantify this, we measured the root-mean-square (RMS) value of the fluctuations in WT and $\alpha6^{L9'S}$ voltage-clamp recordings. There was a significant decrease in the noise for $\alpha6^{L9'S}$ cells in the presence of αCtxMII (Figure 5D). We found no effect of CNQX, picrotoxin, or TTX on the increased membrane noise in $\alpha6^{L9'S}$ cells (Figure S7). DHβE, however, completely eliminated the increased noise similar to αCtxMII (Figure S7). These results further demonstrate that VTA DA neurons express functional, hypersensitive α6* nAChRs and that these receptors may be activated by local ACh.

We examined the properties of hypersensitive α6* receptors in DA neurons of the substantia nigra pars compacta (SNc) and found similar results to the VTA. SNc DA neurons from $\alpha6^{L9'S}$ mice expressed hypersensitive nicotinic currents relative to WT, and firing rates were excited by 1 μM nicotine in $\alpha6^{L9'S}$ but not WT cells (Figures S8A and S8B). Finally, $\alpha6^{L9'S}$ SNc DA neurons expressed tonically active, αCtxMII-sensitive α6* receptors (Figure S8C).

Selective Expression of Functional α6* Receptors in Midbrain DA Neurons

Although expression data suggest selective expression of α6* nAChRs in DA neurons, no electrophysiological experiments supporting this idea have been published. Midbrain DA neurons typically express D2-class autoreceptors, in contrast to midbrain GABAergic neurons (Nashmi et al., 2007). We recorded from 15 VTA neurons, ten of which expressed α6* nAChRs (based on large inward current responses to 1 μM nicotine) and five which

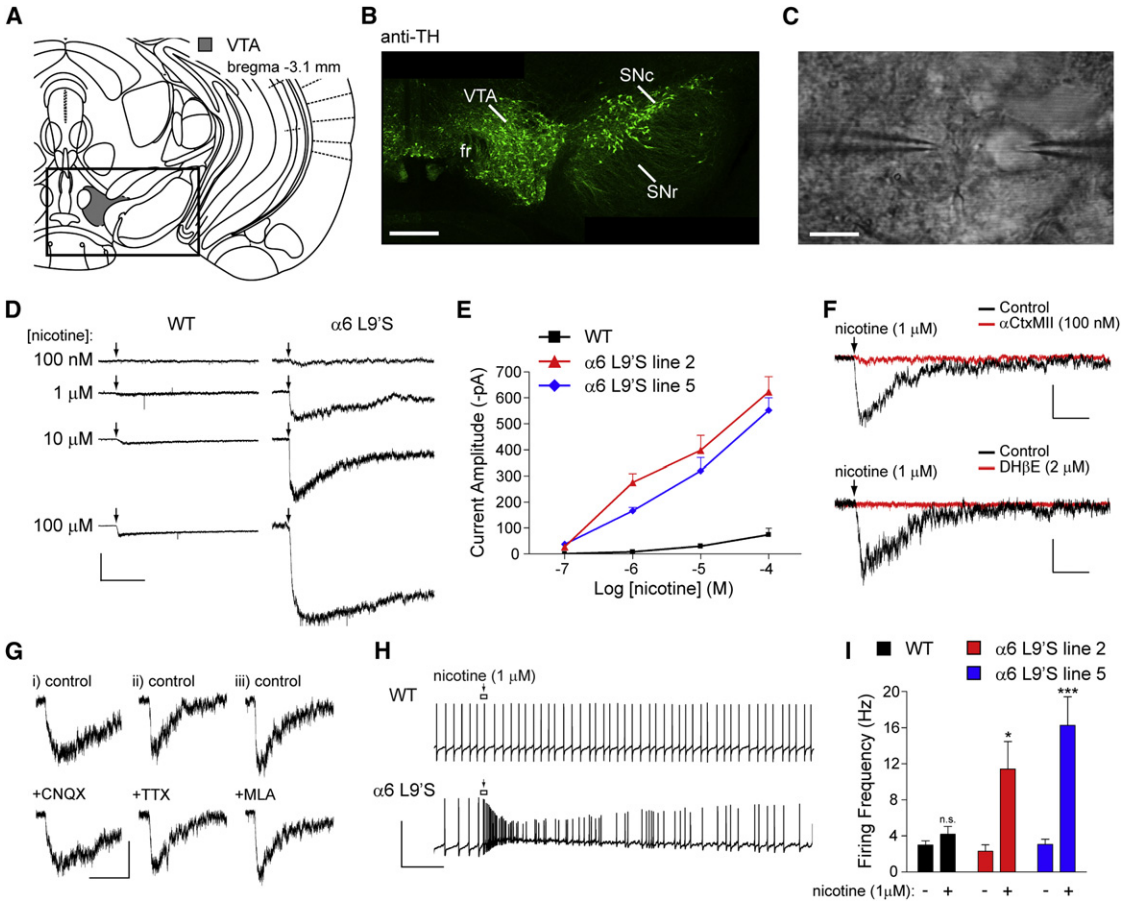

Figure 4. Ventral Tegmental Area DA Neurons Express Hypersensitive nAChRs

(A) Diagram of coronal sections from mouse brain containing ventral tegmental area (Franklin and Paxinos, 2008).

(B) Tyrosine hydroxylase (TH) staining of DA neurons in coronal slices. Coronal slices (250 μm; bregma −3.1 mm) from an $\alpha6^{L9'S}$ mouse were fixed and stained for TH as described in Supplemental Experimental Procedures. The boxed area from (A) is shown. Scale bar: 350 μm.

(C) Micrograph of VTA neuron studied with local nicotine application. A VTA neuron is recorded via the patch pipette (right), and the cell body is stimulated with a nicotine-filled micropipette (left). Scale bar: 20 μm.

(D) Hypersensitive nAChRs in VTA neurons. Patch-clamp recordings were taken from VTA DA neurons in coronal slices from $\alpha6^{L9'S}$ and WT mice. Neurons were voltage clamped at −60 mV, and nicotine at the indicated concentration was locally applied to the cell body using a picospritzer (250 ms). Except during drug application, the micropipette tip was kept several hundred microns from the cell to prevent receptor desensitization. Scale bars: 200 pA, 5 s.

(E) Concentration-response relationship for hypersensitive nicotinic responses in WT and $\alpha6^{L9'S}$ mouse lines. The average peak amplitude of the cellular response for each mouse line and each nicotine concentration is plotted.

(F) Hypersensitive nAChRs are inhibited by αCtxMII and dihydro-β-erythroidine (DHβE). Nicotine (1 μM) was locally applied to VTA DA neurons in $\alpha6^{L9'S}$ slices before (black trace) and after (red trace) 10 min bath application of αCtxMII (100 nM) or DHβE (2 μM) (n = 5 for each antagonist). Scale bars: 100 pA, 3 s.

(G) Hypersensitive nAChR activation is independent of AMPA receptor function, action potentials, and α7* nAChRs. The indicated drug was bath applied to VTA DA neurons in $\alpha6^{L9'S}$ slices, followed by activation of nAChRs with local application of 1 μM nicotine. Peak current amplitudes in the presence of 6-cyano-7-nitro-quinoxaline-2,3-dione (CNQX), tetrodotoxin (TTX), or methyllycaconitine (MLA) were unchanged. Results from both mouse lines were identical in all cells tested (n = 3 for each drug). Scale bars: (Gi) 100 pA, 3 s; (Gii) 60 pA, 3 s; (Giii) 70 pA, 3 s.

(H) Dopamine neuron firing is augmented by a low nicotine concentration only in $\alpha6^{L9'S}$ mice. VTA dopamine neurons were held in I = 0 mode, and nicotine (1 μM) was puff applied (arrow) as in (D) following a stable recording of baseline firing. A representative firing response is shown for a neuron from each genotype. Scale bars: 100 mV, 2 s.

(I) Quantification of firing responses in WT and $\alpha6^{L9'S}$ VTA DA neurons. Peak instantaneous firing frequency values for each nicotine (1 μM) application (one per cell) were derived and averaged for each mouse line. Average peak values are compared with the average baseline firing rate for the same group of cells. Data are reported as mean ± SEM. *p < 0.05, ***p < 0.001.

did not. All cells expressing α6* nAChRs were sensitive to the inhibitory properties of the D2 DA receptor agonist quinpirole (Figure 6A, panel i), indicating that these cells were likely DAergic. In contrast, most α6*-negative cells did not express D2 receptors (Figure 6A, panel ii). To more accurately determine whether α6* receptors are functionally expressed in DA and/or GABA cells in midbrain, we recorded from substantia nigra (SN) neurons in slices from WT and $\alpha6^{L9'S}$ mice. The spatial partitioning of DA and GABA neurons in the SN pars compacta (SNc) and pars reticulata (SNr) (Figure 6B, panel i) was combined with

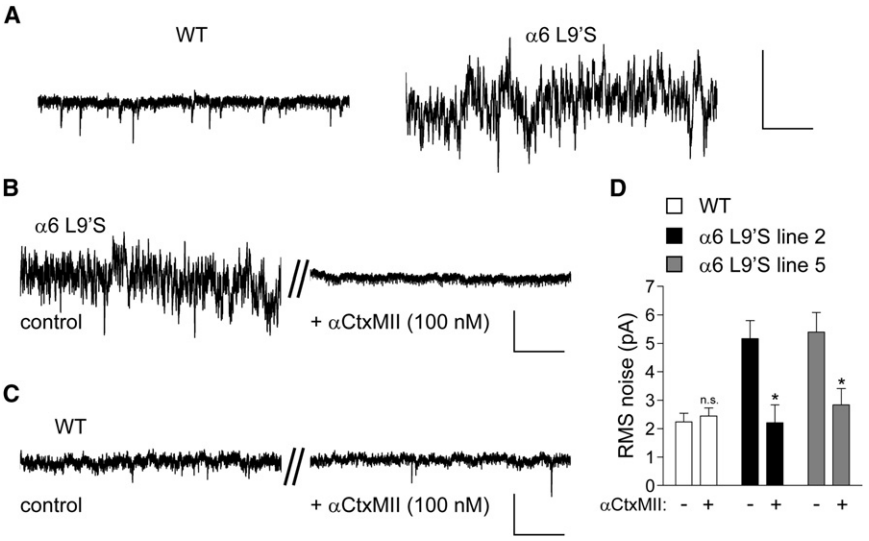

Figure 5. Spontaneous α6 Channel Activity in $\alpha6^{L9'S}$ VTA DA Neurons

(A) Increased current fluctuations in voltage-clamp recordings from $\alpha6^{L9'S}$ neurons. VTA DA neurons from WT or $\alpha6^{L9'S}$ mice were voltage clamped at −60 mV. A segment from a representative voltage-clamp recording is shown. Scale bars: 40 pA, 0.8 s.

(B) Noise in $\alpha6^{L9'S}$ neurons is dependent on α6* nAChRs. VTA DA neurons were voltage clamped at −60 mV, and a baseline recording was taken (control). αCtxMII was bath applied for 10 min, and a representative (n = 4, each line) segment of the voltage-clamp record after this 10 min period is shown (+αCtxMII, 100 nM) for the same cell.

(C) αCtxMII inhibition has no effect in WT control recordings. As a negative control for perfusion artifacts, WT neurons were assayed as in (B).

(D) Quantification of channel noise increase in $\alpha6^{L9'S}$ mice. RMS noise values for voltage-clamp recordings from VTA DA neurons in the presence and absence of αCtxMII are shown.

Data are reported as mean ± SEM. *$p < 0.05$. Scale bars (B and C): 20 pA, 0.5 s.

electrophysiological signatures (Figure 6B, panels ii–iv; see Experimental Procedures) to unambiguously identify these cell types. In whole-cell recordings from $\alpha6^{L9'S}$ and WT SN neurons, we observed hypersensitive nicotinic responses in $\alpha6^{L9'S}$ DA neurons, but not in GABA neurons (Figure 6C). Average peak current amplitudes were comparable between $\alpha6^{L9'S}$ lines 2 and 5 in SNc DA neurons (Figure 6D, panel i). Average responses in WT and $\alpha6^{L9'S}$ GABA neurons were ≤10 pA (Figure 6D, panel ii). Responses to nicotine at 1 μM were undetectable in WT DA and GABA neurons (Figure 6C, panel i); however, these cells responded predictably to 100 μM or 1 mM nicotine (data not shown). As a control for the specificity of our results, we recorded from SNc and SNr neurons in slices from $\alpha4^{L9'A}$ mice. We found hypersensitive nicotinic responses in SNc and SNr neurons from these mice (Figures 6C and 6D), consistent with the idea that α4 is expressed in both DA and GABA cells (Nashmi et al., 2007). These results, coupled with the absence of α6* receptors in GABAergic presynaptic terminals in striatum (Figures 2I–2K), indicate that functional α6* receptors, in contrast to α4* receptors, are restricted to DA neurons in the midbrain.

The results thus far suggest increased DA tone in midbrain and/or striatum. To examine this, we studied pacemaker and nicotine-induced firing of VTA DA neurons in the absence and presence of sulpiride, a D2 DA receptor antagonist. There was no change in the ability of sulpiride to modestly increase baseline firing between WT and $\alpha6^{L9'S}$ VTA DA cells (Figure S9). Further, sulpiride did not affect 1 μM nicotine-induced increases in firing in $\alpha6^{L9'S}$ cells or its lack of effect in WT cells (Figure S9). To determine whether augmented striatal DA release in $\alpha6^{L9'S}$ mice (Figure 2) could be detected in brain slices using patch-clamp recordings, we studied striatal cholinergic interneurons. These cells are readily identifiable (Figure S10A), their activity is modulated by DA, and they are the source of ACh that activates α6* receptors on presynaptic DA terminals. We detected no change in spontaneous firing between WT and $\alpha6^{L9'S}$ cells (Figure S10B). The resting membrane potential for $\alpha6^{L9'S}$ line 2 (but not line 5) was hyperpolarized compared to WT (Figure S10C). Although DA may modulate I_h currents in cholinergic interneurons (Deng et al., 2007), we found no difference between WT and $\alpha6^{L9'S}$ I_h expression or function in these cells (Figures S10D and S10E).

$\alpha6^{L9'S}$ nAChRs in Locus Coeruleus Neurons Do Not Account for Behavioral Phenotypes in Mutant Mice

To determine whether α6* activation in $\alpha6^{L9'S}$ mice might also stimulate locus coeruleus (LC) neuron firing, we recorded from LC neurons in coronal slices from WT and $\alpha6^{L9'S}$ mice (Figure 7A). LC neurons express tyrosine hydroxylase (TH) (Figure 7B), exhibit spontaneous firing (1–2 Hz; Figure 7C, panel i), and lack I_h (Figure 7C, panels ii and iii). LC neurons from $\alpha6^{L9'S}$ mice exhibited larger responses to locally applied nicotine compared to WT cells and cells from $\alpha4^{L9'A}$ knockin mice (Figures 7D and 7E). Although these responses were sensitive to αCtxMII (Figure 7F) and therefore α6 dependent, they were smaller and ~10-fold less sensitive to nicotine than were receptors on VTA DA neurons (compare Figures 4E and 7E). LC neurons were also able to fire action potentials in response to nicotine (Figure 7G), but at concentrations of nicotine 10-fold higher than for DA neurons (Figure 7H). The reduced sensitivity of LC α6* nAChRs relative to receptors on DA neurons suggests that they do not participate in the psychostimulant response to nicotine that we observed. In support of this, we found no change in the locomotor response to nicotine when prazosin (α1AR antagonist) or yohimbine (α2AR antagonist) were administered prior to challenge with nicotine (Figure 1H).

DISCUSSION

$\alpha6^{L9'S}$ Mice Reveal a Role for α6* nAChRs in Cholinergic Modulation of DA Transmission

Here, we report several new aspects of α6* nAChR biology and its role in cholinergic regulation of DA transmission. Also, we show the behavioral effects of selectively activating DA neurons

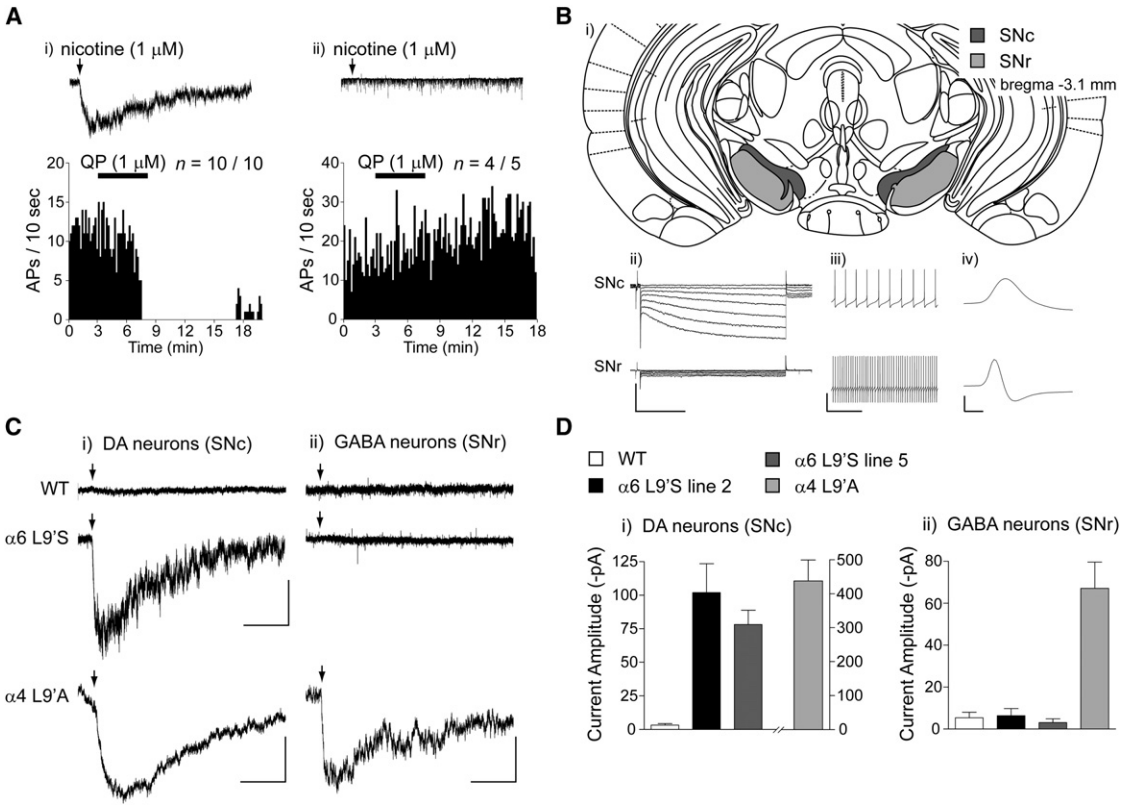

Figure 6. Functional α6* nAChRs Are Selectively Expressed in Midbrain DA, but Not GABA, Neurons

(A) VTA DA neurons expressing hypersensitive α6* nAChRs express dopamine D2-class autoreceptors. VTA DA neurons expressing $\alpha6^{L9'S}$ nAChRs were identified by the presence of large (>100 pA) inward nicotinic currents similar to Figure 4. Following nicotine application, cells were held in I = 0 mode, and quinpirole (QP; 1 μM) was bath applied. Action potential firing in response to QP is shown for a representative neuron expressing (panel [Ai]; n = 10/10) or not expressing (panel [Aii]; n = 4/5) $\alpha6^{L9'S}$ receptors.

(B) Identification of substantia nigra (SN) DA and GABA neurons. A diagram of coronal sections (bregma −3.1 mm) from mouse brain containing SN pars compacta (SNc) and pars reticulata (SNr) is shown (Franklin and Paxinos, 2008). SN DA versus GABA neurons were identified by (Bi) location: SNc contains DA neurons whereas SNr is largely GABAergic; (Bii) DA neurons express hyperpolarization-activated cation current (I_h); (Biii) DA neurons exhibit pacemaker firing (1–5 Hz), whereas GABA neurons fire at >10 Hz; (Biv) DA neurons have broad spikes (>2 ms), whereas GABA neurons have narrow (≤1 ms) spikes. Scale bars: (Bii) 400 pA (current traces)/30 mV (voltage step), 0.5 s; (Biii) 50 mV, 1 s; (Biv) 50 mV, 1 ms.

(C) Hypersensitive α6* nAChRs reveal selective expression in DA neurons. SN DA and GABA neurons were identified according to criteria in (B). Neurons in slices from WT, $\alpha6^{L9'S}$, and $\alpha4^{L9'A}$ mice were patch clamped in whole-cell configuration, and nicotine (1 μM) was locally applied (arrow) to activate hypersensitive nAChRs. Representative recordings for each are shown. Scale bars: (WT and $\alpha6^{L9'S}$) 100 pA, 5 s; ($\alpha4^{L9'A}$) 200 pA (DA)/80 pA (GABA), 5 s.

(D) Quantification of current amplitudes from (C). Average peak current amplitude in response to 1 μM nicotine for each genotype and cell type is shown. Data are expressed as mean ± SEM.

(Figure 1). Our electrophysiology and neurochemistry experiments reveal a major role for α6* nAChRs in regulating both DA neuron firing (Figures 4 and S8) and synaptic release of DA in the striatum (Figures 2 and 3). Our finding that α6* nAChRs are largely excluded from midbrain GABA neurons (Figure 6) and from striatal GABAergic terminals (Figures 2I–2K), in stark contrast to α4β2* nAChRs, is sustained by our behavioral data suggesting relatively unrestrained DA transmission in $\alpha6^{L9'S}$ mutant mice. We propose a model in which specific functional expression of high-sensitivity $\alpha6^{L9'S}$ nAChRs in DA neurons renders these cells selectively hypersensitive (Figure S11) to activation by endogenous ACh (Figure 8B) or by exogenous nicotine (Figure 8D). This likely reflects that, in WT mice or in humans, high-affinity α6* nAChRs are specifically poised to modulate the activity of monoamine neurotransmitters such as DA. These studies provide long-sought sufficiency data for α6* nAChRs, complementing studies utilizing α6* loss-of-function mutations and pharmacological blockade.

In Vivo α6* nAChR Stoichiometry and Biophysical Properties Revealed by $\alpha6^{L9'S}$ Mice

We observed similar levels of αCtxMII binding in $\alpha6^{L9'S}$ brains compared to WT controls (Figures S1F and S1G). This is interesting in light of the fact that the two $\alpha6^{L9'S}$ lines harbor multiple copies of the transgene (Figure S1D). Unlike an exon-replacement knockin approach, $\alpha6^{L9'S}$ BAC transgenic mice retain two copies of WT *Chrna6*. In DA neurons, α6 and α4 subunits compete for common, limiting nAChR subunits such as β2, possibly β3 and α5, and probably for unknown assembly factors or chaperone proteins that may be specific to this cell type. As a result,

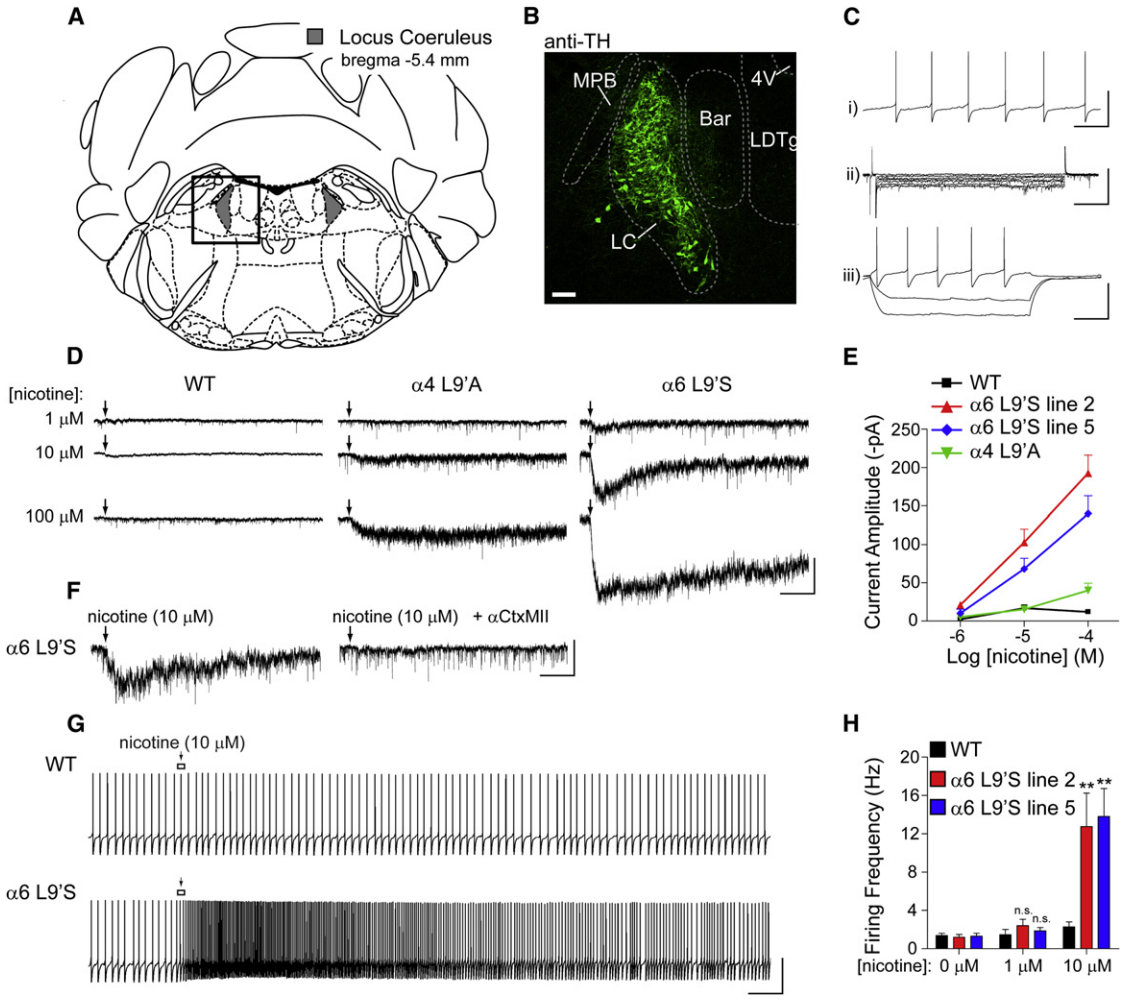

Figure 7. Modest Hypersensitivity to Nicotine at $\alpha6^{L9'S}$ nAChRs in Noradrenergic Locus Coeruleus Neurons

(A) Diagram of coronal sections (bregma −5.4 mm) containing locus coeruleus (Franklin and Paxinos, 2008).

(B) Tyrosine hydroxylase (TH) staining of NE neurons in coronal slices. Coronal slices (200 μm; bregma −5.4 mm) from an $\alpha6^{L9'S}$ mouse were fixed and stained for TH as described in Supplemental Experimental Procedures. The boxed area from (A) is shown. Scale bar: 100 μm. MPB, medial parabrachial nucleus; LC, locus coeruleus; Bar, Barrington's nucleus; LDTg, laterodorsal tegmental nucleus; 4V, fouth ventricle.

(C) Electrophysiological identification of LC neurons. LC neurons are identified by (Ci) pacemaker firing at 1–2 Hz, (Cii) lack of I_h, and (Ciii) lack of membrane potential "sag" for hyperpolarizing current pulses (responses shown for injection of −80, −40, and +20 pA). Scale bars: (Ci) 70 mV, 1.5 s; (Cii) 150 pA, 350 ms; (Ciii) 70 mV, 500 ms.

(D) Hypersensitive nicotinic responses in LC neurons. Patch-clamp recordings were taken from LC neurons in coronal slices from WT, $\alpha4^{L9'A}$, and $\alpha6^{L9'S}$ mice. Neurons were voltage clamped at −60 mV, and nicotine at the indicated concentration was locally applied (arrow) to the cell body (250 ms).

(E) Concentration-response relationship for hypersensitive nicotinic responses in WT, $\alpha4^{L9'A}$, and $\alpha6^{L9'S}$ mice. The average peak amplitude of the cellular response for each mouse line and each nicotine concentration is plotted.

(F) Hypersensitive $\alpha6^{L9'S}$ nAChRs are inhibited by αCtxMII. Nicotine (10 μM) was locally applied (arrow) to LC neurons in $\alpha6^{L9'S}$ slices before and after 10 min bath application of αCtxMII (100 nM) (n = 3). Scale bars: 50 pA, 4 s.

(G) Noradrenergic neuron firing is augmented by a moderate nicotine concentration only in $\alpha6^{L9'S}$ mice. Following a stable recording of baseline action potential firing, nicotine (10 μM) was puff applied (arrow) as in (D). Exemplar responses are shown for a WT and $\alpha6^{L9'S}$ neuron. Scale bars: 70 mV, 3 s.

(H) Quantification of firing responses in WT and $\alpha6^{L9'S}$ LC neurons. Peak instantaneous firing frequency values for each nicotine concentration were derived and averaged. Average peak values are compared with the average baseline firing rate (0 μM nicotine) for the same group of cells.

Data are reported as mean ± SEM. **p < 0.01.

the level of functional α6* expression in $\alpha6^{L9'S}$ neurons is determined by a competition between WT and L9′S α6 subunits. Indeed, for every agonist tested, we observed diminished peak αCtxMII-resistant (α4β2* dependent) DA release in $\alpha6^{L9'S}$ ST/OT (Figures 2 and 3) despite equal levels of α4β2*-binding sites (Figure S1G). Future crosses of $\alpha6^{L9'S}$ mice to α4, β2, and β3 nAChR heterozygous or homozygous KO mice will yield further insights into nAChR subunit stoichiometry in vivo.

We noted a large increase in the potency and efficacy of nicotine in whole-cell recordings from $\alpha6^{L9'S}$ DA neurons (Figures 4D

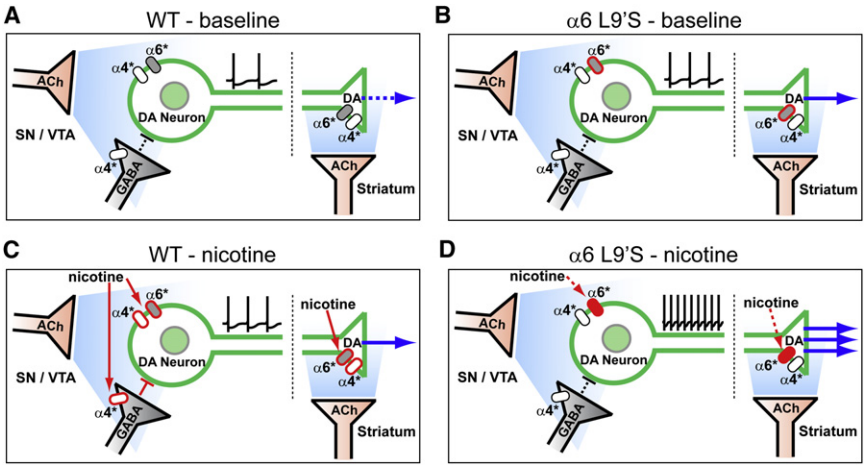

Figure 8. Hypersensitive DA Neurons Alter Basal Ganglia Circuitry for Cholinergic Transmission and Responses to Nicotine

(A–D) Schematic for baseline and nicotine-induced activation of DA neurons. In WT mice, background (A) ACh weakly stimulates somatic and presynaptic α4* and α6* nAChRs, leading to tonic DA release in ST. In $\alpha6^{L9'S}$ mice, baseline ACh (B) activation of α6* nAChRs may cause heightened DA release via increased somatic and presynaptic nAChR activity. In WT (C), systemic nicotine (≥0.5 mg/kg, i.p.) activates α4* and α6* nAChRs on DA neurons, and α4* nAChRs on GABA neurons/terminals in midbrain. This, coupled with activation of presynaptic α4* and α6* nAChRs, increases DA release in ST. In $\alpha6^{L9'S}$ mice (D), systemic nicotine (≤0.15 mg/kg, i.p.) specifically activates somatic and presynaptic α6* nAChRs on DA neurons without activating α4* nAChRs on inhibitory GABAergic inputs, which strongly stimulates DA release.

and 4E). With respect to nicotinic channel engineering, the present studies are analogous to electrophysiological and Ca^{2+} flux-based measurements of hypersensitive nicotinic responses in $\alpha4^{L9'S}$, $\alpha4^{L9'A}$, and $\alpha7^{L9'T}$ knockin mice (Fonck et al., 2005; Labarca et al., 2001; Tapper et al., 2004; Wooltorton et al., 2003). The augmented responses (increased efficacy) to agonist likely reflect an increased maximal probability of channel opening, P_{open}, conferred by the L9′S mutation (Labarca et al., 1995), while the increased potency results from this mutation shifting the agonist concentration-response relation to lower concentrations (Revah et al., 1991). The increased noise in voltage-clamp recordings from $\alpha6^{L9'S}$ neurons probably arises from one of two effects: (1) the presence of ACh in the slice preparation that is secreted from terminals of severed mesopontine cholinergic axons or (2) unliganded openings. Future in vivo studies, such as recordings from awake, behaving animals, will help confirm whether $\alpha6^{L9'S}$ mouse spontaneous behavioral phenotypes are caused by the former or the latter.

Contrasting Cell-Specific Expression of α4* versus α6* nAChRs Leads to Behavioral Differences in α4 and α6 Gain-of-Function Mutant Mice

$\alpha6^{L9'S}$ mice are viable and fertile, whereas full expression of $\alpha4^{L9'S}$* receptors causes neonatal lethality due to excitotoxic death of DA neurons (Labarca et al., 2001). This could be due to differential expression of α4 and α6 in development; unlike α4 expression, peak α6 expression occurs well after birth (Azam et al., 2007). It is also possible that $\alpha6^{L9'S}$* receptors are comparatively insensitive to activation by choline at concentrations found in CSF.

In the mesostriatal and mesolimbic DA system, α4β2* nAChRs are expressed in DA neuron cell bodies, dendrites, and axon terminals, as well as in cell bodies and axon terminals of midbrain and striatal GABAergic neurons. Conclusive evidence for α6* nAChR expression, however, is restricted to DA neuron cell bodies and axon terminals. Our present results show that, in midbrain, manipulating α6* nAChR sensitivity affects only DA neurons (Figures S11, 8B, and 8D), whereas sensitized α4* receptors simultaneously increase the sensitivity of DA neurons and their inhibitory GABAergic inputs (Figures 6, 8A, and 8C). This circuit-level difference explains a distinction between the locomotor effects of nicotine in the two gain-of-function mouse strains. WT mice display a hypolocomotor response to nicotine, and $\alpha4^{L9'A}$ mice recapitulate the WT response, only at much lower doses (Tapper et al., 2007). On the other hand, $\alpha6^{L9'S}$ mice exhibit a sign change: psychomotor stimulation by nicotine (Figure 1F).

This cell-type difference in expression between α4 and α6 nAChR subunits may also lead to the behavioral differences between $\alpha4^{L9'A}$ and $\alpha6^{L9'S}$ mice in response to repeated nicotine injections. Repeated, selective activation of α4* nAChRs produces locomotor sensitization (Tapper et al., 2004, 2007), whereas repeated activation of α6* nAChRs produces neither tolerance nor sensitization (Figure 1I). Locomotor sensitization may require nicotinic activation of GABAergic transmission, which is afforded by α4* nAChRs but not α6* nAChRs (Nashmi et al., 2007). Alternatively, the mechanism of sensitization could involve nAChR upregulation, to which α4β2* receptors are particularly prone (Nguyen et al., 2003) but to which α6* receptors are apparently resistant (Perry et al., 2007).

α6* nAChRs Preferentially Modulate the Mesolimbic versus Mesostriatal DA System

The VTA and NAc (mesolimbic DA pathway) are key mediators of the addictive properties of nicotine (Corrigall et al., 1994), and a recent report using pharmacological blockade suggests that α6* nAChRs specifically mediate cholinergic modulation of DA release in NAc (Exley et al., 2007). Our results support this in two ways: (1) we observe greater expression of α6* currents in VTA versus SNc neurons (compare Figures 4E, 6D, and S8A), and (2) DA release is more strongly controlled by α6* on VTA-derived terminals versus SNc-derived terminals (compare EC_{50} values in Figures 2G and 2H). Although we cannot completely distinguish the contribution of dorsal versus ventral striatum in our behavioral experiments, our DA release data suggest that the first α6* nAChRs significantly activated by nicotine are those in the mesolimbic pathway.

VTA β2* nAChRs are critical mediators of exploratory behavior in mice (Granon et al., 2003; Maskos et al., 2005). The VTA is

important for curiosity or the response to novelty, perhaps by responding to cholinergic excitation to mediate the switch to burst firing in DA neurons. If VTA β2* nAChRs are necessary for normal responses to novelty, then it is not surprising that sensitized VTA β2* nAChRs such as $\alpha6^{L9'S}\beta2^*$ in mutant mice render the animals hypersensitive to novelty (Figures 1C and 1D). This phenotype is much smaller or absent in $\alpha4^{L9'A}$ mice, reflecting the relative importance of selectively activating DA in eliciting this response.

$\alpha6^{L9'S}$ Mice Reveal a Role for Cholinergic Transmission in Behavioral Hyperactivity

In midbrain, ACh released from mesopontine cholinergic terminals acts on DA neuron nAChRs in vivo (Mameli-Engvall et al., 2006) (Figure 8A). α6* nAChRs have the highest known sensitivity to ACh, making them excellent candidates to mediate the stimulatory action of endogenous ACh on DA neurons. The tonic activation of α6* nAChRs that we observe in midbrain slices is likely due to endogenous ACh. Although we observe no difference in DA neuron baseline firing in vitro (Figures 4I and S8B), tonic midbrain α6* nAChR activation may be sufficient in vivo to contribute to behavioral phenotypes in $\alpha6^{L9'S}$ mice. In striatum, tonic extracellular DA is controlled by presynaptic nAChRs via continuous, low-level ACh released from cholinergic interneurons (Zhou et al., 2001). This acts to maintain a high probability of DA release from the terminal during tonic firing (Rice and Cragg, 2004; Zhang and Sulzer, 2004). Sensitization of α6* nAChRs (in $\alpha6^{L9'S}$ mice) likely modifies DA release at presynaptic terminals in addition to effects at DA neuron cell bodies; DA terminals with $\alpha6^{L9'S}$ channels presumably have a decreased failure rate for single spike-induced release. This is supported by in vitro electrochemical studies of α6*-dependent DA release (Exley et al., 2007). Thus, genetic sensitization of DA neurons to ACh in midbrain and facilitation of DA release in striatum (Figure 8B) could easily account for the home cage hyperactivity and the sustained hyperactivity of $\alpha6^{L9'S}$ mutant mice when placed in a novel environment. These phenotypes are reminiscent of DA transporter knockdown mice, which also show hyperactivity and impaired response habituation (Zhuang et al., 2001). Although α6*-regulated norepinephrine (NE) release does not contribute to nicotine psychomotor activation (Figure 1H), our results do not rule out a role for NE in $\alpha6^{L9'S}$ spontaneous hyperactivity. Future studies on the mechanisms of $\alpha6^{L9'S}$ mouse hyperactivity could be useful in understanding the causes of human hyperactivity, such as that observed in ADHD.

In $\alpha6^{L9'S}$ mice, low-dose nicotine stimulates psychomotor activation similar to amphetamine in WT animals (Figure 1E). Nicotine thus recapitulates the spontaneous hyperactivity we observe, though with different kinetics. The difference in response magnitude and duration between responses to novelty and responses to nicotine may reflect different agonist concentration and desensitization kinetics. After ACh is released from nerve terminals, it is hydrolyzed by acetylcholinesterase (AChE), which has a turnover rate of 10^4/s (Wathey et al., 1979) and is abundant in DAergic areas. ACh may not reach concentrations, or remain long enough, to significantly desensitize α6* nAChRs, perhaps even those with mutant L9′S subunits. In contrast, nicotine is eliminated with a half-life of ~7 min (Matta et al., 2007)—nearly 10^7 times longer—and can therefore desensitize receptors, especially β2* nAChRs (Mansvelder et al., 2002). Bolus injections of nicotine in $\alpha6^{L9'S}$ mice potently activate mutant receptors, and the locomotor response decay kinetics could therefore be dominated by both receptor desensitization and metabolic breakdown of nicotine.

Therapeutic Targeting of DA Disorders with α6* nAChRs

The cholinergic system is targeted by several drugs used to treat neural disorders such as Alzheimer's disease and Parkinson's disease (PD). There is a well-documented inverse correlation between smoking and PD (Ritz et al., 2007), and other disorders that can be treated with DA drugs (ADHD, schizophrenia) are associated with a high incidence of smoking (de Leon et al., 1995; Pomerleau et al., 1995). These findings suggest the important role played by the cholinergic system in DA transmission. Our results show that a sensitized response in DA neurons to endogenous ACh may cause a behaviorally relevant state of excess DA. Manipulations to decrease α6* nAChR function may, therefore, be a useful treatment for human disorders involving excess DA. This could be in the form of a competitive antagonist or via viral gene therapy designed to eliminate α6* activity. On the other hand, patients with PD (low DA) may be aided by α6* agonists or allosteric modulators to augment DA release from residual DA terminals (Quik and McIntosh, 2006). Our data clearly show that an α6-selective compound potently stimulates both DA release and locomotor activity (Figure 3). Further, the absence of sensitization or tolerance to repeated α6* activation (Figure 1I) suggests that clinical α6* agonists may have reduced abuse liability. Unlike L-DOPA or direct DA receptor agonists/antagonists, compounds manipulating DA neuron firing by targeting α6* nAChRs might avoid well known use-dependent side effects such as dyskinesias.

EXPERIMENTAL PROCEDURES

Bacterial Artificial Chromosome Recombineering and Transgenesis

For a complete description of the methods used for recombineering and transgenesis, see Supplemental Data. A bacterial artificial chromosome (BAC), RP24-149I12, containing the mouse α6 nicotinic receptor subunit gene (*Chrna6*) was obtained from the BACPAC Resource Center (BPRC) at Children's Hospital Oakland Research Institute (Oakland, CA). BAC recombineering was carried out using a Counter Selection BAC modification kit (Genebridges; Heidelberg, Germany). α6 nAChR Leucine 280 (Leu9′) was mutated to a serine using a two-step selection/counterselection protocol. First, a 15 bp stretch of *Chrna6* exon 5 containing the coding sequence for V278 through L282 was replaced with a cassette containing a tandem selection (neo)/counterselection (rpsL) marker. Neo was used to select positive recombinants, and an engineered NotI restriction site pair flanking the selection cassette was used to confirm the location of the exogenously inserted DNA within the BAC. In the second step, *Chrna6* exon 5 was restored using counterselection. Bacterial cells were placed under selective pressure (via streptomycin sensitivity gained by insertion of the rpsL marker) to lose the neo-rpsL cassette and replace it with nonselectable DNA engineered to insert the Leu9′ to Ser (L280S) mutation. The resultant strain harbored a BAC with no ectopic DNA in or around *Chrna6*.

Injection-grade $\alpha6^{L9'S}$ BAC DNA was prepared via double CsCl banding (Lofstrand Labs; Gaithersberg, MD). To produce transgenic animals, BAC DNA was injected into the male pronucleus of recently fertilized FVB/N embryos and implanted into pseudopregnant Swiss-Webster surrogates. Transgenic founders were identified using tail biopsy DNA and PCR primers designed to detect the L9′S mutation. Founders were crossed to C57BL/6J

(Jackson Labs; Bar Harbor, ME) to obtain germline transmission and to establish a colony, and transgenic mice were continually backcrossed to C57BL/6J.

Locomotor Activity

Locomotor activity was assayed similar to Fonck et al. (2005) and is described in Supplemental Data.

Neurotransmitter Release from Striatal Synaptosomes

DA and GABA release from striatal synaptosomes was carried out similar to Grady et al. (2002) and Nashmi et al. (2007) and is described in Supplemental Data.

Patch-Clamp Electrophysiology

Methods for patch-clamp recordings are completely detailed in Supplemental Data. Transgenic and nontransgenic mice (midbrain, P17–P25; locus coeruleus, P21–P28; striatum, P42–P56) were anesthetized, followed by cardiac perfusion with oxygenated (95% O_2/5% CO_2) ice-cold glycerol-based artificial CSF (gACSF). Coronal slices (midbrain, striatum: 250 μm; pons: 200 μm) were cut and allowed to recover for at least 1 hr at 32°C in regular, oxygenated artificial CSF (ACSF). Somatic recordings from visually identified midbrain, pontine, or striatal neurons were obtained using patch electrodes filled with internal pipette solution containing 135 mM potassium gluconate, 5 mM EGTA, 0.5 mM $CaCl_2$, 2 mM $MgCl_2$, 10 mM HEPES, 2 mM Mg-ATP, and 0.1 mM GTP. Recordings were taken at 32°C with an Axopatch 1D amplifier, a 16 bit Digidata 1322A A/D converter, and pCLAMP9.2 software (all Molecular Devices Axon; Sunnyvale, CA). For nicotine application, a drug-filled micropipette was used to locally apply nicotine using pressure application. A piezoelectric translator rapidly moved the nicotine-filled pipette close to and away from the cell to avoid nAChR desensitization.

Immunohistochemistry and Spectral Confocal Imaging

Coronal brain slices cut for patch-clamp recording were processed similar to Lerchner et al. (2007) and stained according to Drenan et al. (2005). Spectral confocal imaging was similar to Drenan et al. (2008). See Supplemental Data for more details.

SUPPLEMENTAL DATA

The Supplemental Data include Supplemental Experimental Procedures, Figures, and Tables and can be found with this article online at http://www.neuron.org/supplemental/S0896-6273(08)00756-3.

ACKNOWLEDGMENTS

We thank members of the Lester lab for helpful discussions. Special thanks to B. Drenan. Thanks to C. Wageman, E. Myers, C. Xiao, A. Tapper, R. Nashmi, C. Fonck, J. Schwarz, J. Jankowsky, M. Liu, P. Deshpande, S. Benazouz, and C. Zhou. This work was supported by H.H.M.I. (N.H., J.M. Miwa, S.B.) and grants from NIH (DA09121, DA17279, and NS11756 to H.A.L.; DA19375 to H.A.L. and M.J.M.; DA03194 to M.J.M.; DA12242 to M.J.M. and P.W.; MH53631 and GM48677 to J.M. McIntosh), the Moore Foundation, the Croll Research Foundation (to J.M. Miwa) and the California Tobacco Related Disease Research Program (TRDRP; 12RT-0245 to H.A.L.). R.M.D. was supported by postdoctoral fellowships from TRDRP (15FT-0030) and NIH (DA021492 and NS007251).

Accepted: September 4, 2008
Published: October 8, 2008

REFERENCES

Azam, L., and McIntosh, J.M. (2006). Characterization of nicotinic acetylcholine receptors that modulate nicotine-evoked [^{3}H]norepinephrine release from mouse hippocampal synaptosomes. Mol. Pharmacol. *70*, 967–976.

Azam, L., Winzer-Serhan, U.H., Chen, Y., and Leslie, F.M. (2002). Expression of neuronal nicotinic acetylcholine receptor subunit mRNAs within midbrain dopamine neurons. J. Comp. Neurol. *444*, 260–274.

Azam, L., Chen, Y., and Leslie, F.M. (2007). Developmental regulation of nicotinic acetylcholine receptors within midbrain dopamine neurons. Neuroscience *144*, 1347–1360.

Bencherif, M., Lovette, M.E., Fowler, K.W., Arrington, S., Reeves, L., Caldwell, W.S., and Lippiello, P.M. (1996). RJR-2403: a nicotinic agonist with CNS selectivity I. In vitro characterization. J. Pharmacol. Exp. Ther. *279*, 1413–1421.

Bhatti, B.S., Strachan, J.P., Breining, S.R., Miller, C.H., Tahiri, P., Crooks, P.A., Deo, N., Day, C.S., and Caldwell, W.S. (2008). Synthesis of 2-(pyridin-3-yl)-1-azabicyclo[3.2.2]nonane, 2-(pyridin-3-yl)-1-azabicyclo[2.2.2]octane, and 2-(pyridin-3-yl)-1-azabicyclo[3.2.1]octane, a class of potent nicotinic acetylcholine receptor-ligands. J. Org. Chem. *73*, 3497–3507.

Calabresi, P., Lacey, M.G., and North, R.A. (1989). Nicotinic excitation of rat ventral tegmental neurones in vitro studied by intracellular recording. Br. J. Pharmacol. *98*, 135–140.

Cartier, G.E., Yoshikami, D., Gray, W.R., Luo, S., Olivera, B.M., and McIntosh, J.M. (1996). A new alpha-conotoxin which targets α3β2 nicotinic acetylcholine receptors. J. Biol. Chem. *271*, 7522–7528.

Champtiaux, N., Han, Z.Y., Bessis, A., Rossi, F.M., Zoli, M., Marubio, L., McIntosh, J.M., and Changeux, J.P. (2002). Distribution and pharmacology of α6-containing nicotinic acetylcholine receptors analyzed with mutant mice. J. Neurosci. *22*, 1208–1217.

Champtiaux, N., Gotti, C., Cordero-Erausquin, M., David, D.J., Przybylski, C., Lena, C., Clementi, F., Moretti, M., Rossi, F.M., Le Novere, N., et al. (2003). Subunit composition of functional nicotinic receptors in dopaminergic neurons investigated with knock-out mice. J. Neurosci. *23*, 7820–7829.

Corrigall, W.A., Coen, K.M., and Adamson, K.L. (1994). Self-administered nicotine activates the mesolimbic dopamine system through the ventral tegmental area. Brain Res. *653*, 278–284.

Cui, C., Booker, T.K., Allen, R.S., Grady, S.R., Whiteaker, P., Marks, M.J., Salminen, O., Tritto, T., Butt, C.M., Allen, W.R., et al. (2003). The β3 nicotinic receptor subunit: a component of α-Conotoxin MII-binding nicotinic acetylcholine receptors that modulate dopamine release and related behaviors. J. Neurosci. *23*, 11045–11053.

de Leon, J., Dadvand, M., Canuso, C., White, A.O., Stanilla, J.K., and Simpson, G.M. (1995). Schizophrenia and smoking: an epidemiological survey in a state hospital. Am. J. Psychiatry *152*, 453–455.

Deng, P., Zhang, Y., and Xu, Z.C. (2007). Involvement of I_h in dopamine modulation of tonic firing in striatal cholinergic interneurons. J. Neurosci. *27*, 3148–3156.

Drenan, R.M., Doupnik, C.A., Boyle, M.P., Muglia, L.J., Huettner, J.E., Linder, M.E., and Blumer, K.J. (2005). Palmitoylation regulates plasma membrane-nuclear shuttling of R7BP, a novel membrane anchor for the RGS7 family. J. Cell Biol. *169*, 623–633.

Drenan, R.M., Nashmi, R., Imoukhuede, P., Just, H., McKinney, S., and Lester, H.A. (2008). Subcellular trafficking, pentameric assembly, and subunit stoichiometry of neuronal nicotinic acetylcholine receptors containing fluorescently labeled α6 and β3 subunits. Mol. Pharmacol. *73*, 27–41.

Exley, R., Clements, M.A., Hartung, H., McIntosh, J.M., and Cragg, S.J. (2007). α6-containing nicotinic acetylcholine receptors dominate the nicotine control of dopamine neurotransmission in nucleus accumbens. Neuropsychopharmacology *33*, 2158–2166.

Fonck, C., Cohen, B.N., Nashmi, R., Whiteaker, P., Wagenaar, D.A., Rodrigues-Pinguet, N., Deshpande, P., McKinney, S., Kwoh, S., Munoz, J., et al. (2005). Novel seizure phenotype and sleep disruptions in knock-in mice with hypersensitive α4* nicotinic receptors. J. Neurosci. *25*, 11396–11411.

Franklin, K.B.J., and Paxinos, G. (2008). The Mouse Brain in Stereotaxic Coordinates, Third Edition (New York, NY: Elsevier, Inc.).

Gotti, C., Moretti, M., Clementi, F., Riganti, L., McIntosh, J.M., Collins, A.C., Marks, M.J., and Whiteaker, P. (2005a). Expression of nigrostriatal α6-containing nicotinic acetylcholine receptors is selectively reduced, but not eliminated, by β3 subunit gene deletion. Mol. Pharmacol. *67*, 2007–2015.

Gotti, C., Moretti, M., Zanardi, A., Gaimarri, A., Champtiaux, N., Changeux, J.P., Whiteaker, P., Marks, M.J., Clementi, F., and Zoli, M. (2005b). Heterogeneity and selective targeting of neuronal nicotinic acetylcholine receptor (nAChR)

subtypes expressed on retinal afferents of the superior colliculus and lateral geniculate nucleus: identification of a new native nAChR subtype α3β2(α5 or β3) enriched in retinocollicular afferents. Mol. Pharmacol. *68*, 1162–1171.

Grady, S.R., Murphy, K.L., Cao, J., Marks, M.J., McIntosh, J.M., and Collins, A.C. (2002). Characterization of nicotinic agonist-induced [^{3}H]dopamine release from synaptosomes prepared from four mouse brain regions. J. Pharmacol. Exp. Ther. *301*, 651–660.

Granon, S., Faure, P., and Changeux, J.P. (2003). Executive and social behaviors under nicotinic receptor regulation. Proc. Natl. Acad. Sci. USA *100*, 9596–9601.

Grenhoff, J., Aston-Jones, G., and Svensson, T.H. (1986). Nicotinic effects on the firing pattern of midbrain dopamine neurons. Acta Physiol. Scand. *128*, 351–358.

Kaiser, S.A., Soliakov, L., Harvey, S.C., Luetje, C.W., and Wonnacott, S. (1998). Differential inhibition by α-conotoxin-MII of the nicotinic stimulation of [^{3}H]dopamine release from rat striatal synaptosomes and slices. J. Neurochem. *70*, 1069–1076.

Kulak, J.M., Nguyen, T.A., Olivera, B.M., and McIntosh, J.M. (1997). α-conotoxin MII blocks nicotine-stimulated dopamine release in rat striatal synaptosomes. J. Neurosci. *17*, 5263–5270.

Labarca, C., Nowak, M.W., Zhang, H., Tang, L., Deshpande, P., and Lester, H.A. (1995). Channel gating governed symmetrically by conserved leucine residues in the M2 domain of nicotinic receptors. Nature *376*, 514–516.

Labarca, C., Schwarz, J., Deshpande, P., Schwarz, S., Nowak, M.W., Fonck, C., Nashmi, R., Kofuji, P., Dang, H., Shi, W., et al. (2001). Point mutant mice with hypersensitive α4 nicotinic receptors show dopaminergic deficits and increased anxiety. Proc. Natl. Acad. Sci. USA *98*, 2786–2791.

Lanca, A.J., Adamson, K.L., Coen, K.M., Chow, B.L., and Corrigall, W.A. (2000). The pedunculopontine tegmental nucleus and the role of cholinergic neurons in nicotine self-administration in the rat: a correlative neuroanatomical and behavioral study. Neuroscience *96*, 735–742.

Le Novere, N., Zoli, M., and Changeux, J.P. (1996). Neuronal nicotinic receptor α6 subunit mRNA is selectively concentrated in catecholaminergic nuclei of the rat brain. Eur. J. Neurosci. *8*, 2428–2439.

Lerchner, W., Xiao, C., Nashmi, R., Slimko, E.M., van Trigt, L., Lester, H.A., and Anderson, D.J. (2007). Reversible silencing of neuronal excitability in behaving mice by a genetically targeted, ivermectin-gated Cl^- channel. Neuron *54*, 35–49.

Lippiello, P.M., Bencherif, M., Gray, J.A., Peters, S., Grigoryan, G., Hodges, H., and Collins, A.C. (1996). RJR-2403: a nicotinic agonist with CNS selectivity II. In vivo characterization. J. Pharmacol. Exp. Ther. *279*, 1422–1429.

Lu, Y., Grady, S., Marks, M.J., Picciotto, M., Changeux, J.P., and Collins, A.C. (1998). Pharmacological characterization of nicotinic receptor-stimulated GABA release from mouse brain synaptosomes. J. Pharmacol. Exp. Ther. *287*, 648–657.

Mameli-Engvall, M., Evrard, A., Pons, S., Maskos, U., Svensson, T.H., Changeux, J.P., and Faure, P. (2006). Hierarchical control of dopamine neuron-firing patterns by nicotinic receptors. Neuron *50*, 911–921.

Mansvelder, H.D., and McGehee, D.S. (2000). Long-term potentiation of excitatory inputs to brain reward areas by nicotine. Neuron *27*, 349–357.

Mansvelder, H.D., Keath, J.R., and McGehee, D.S. (2002). Synaptic mechanisms underlie nicotine-induced excitability of brain reward areas. Neuron *33*, 905–919.

Maskos, U., Molles, B.E., Pons, S., Besson, M., Guiard, B.P., Guilloux, J.P., Evrard, A., Cazala, P., Cormier, A., Mameli-Engvall, M., et al. (2005). Nicotine reinforcement and cognition restored by targeted expression of nicotinic receptors. Nature *436*, 103–107.

Matta, S.G., Balfour, D.J., Benowitz, N.L., Boyd, R.T., Buccafusco, J.J., Caggiula, A.R., Craig, C.R., Collins, A.C., Damaj, M.I., Donny, E.C., et al. (2007). Guidelines on nicotine dose selection for in vivo research. Psychopharmacology (Berl.) *190*, 269–319.

McIntosh, J.M., Azam, L., Staheli, S., Dowell, C., Lindstrom, J.M., Kuryatov, A., Garrett, J.E., Marks, M.J., and Whiteaker, P. (2004). Analogs of α-Conotoxin MII are selective for α6-containing nicotinic acetylcholine receptors. Mol. Pharmacol. *65*, 944–952.

Nashmi, R., Xiao, C., Deshpande, P., McKinney, S., Grady, S.R., Whiteaker, P., Huang, Q., McClure-Begley, T., Lindstrom, J.M., Labarca, C., et al. (2007). Chronic nicotine cell specifically upregulates functional α4* nicotinic receptors: basis for both tolerance in midbrain and enhanced long-term potentiation in perforant path. J. Neurosci. *27*, 8202–8218.

Nguyen, H.N., Rasmussen, B.A., and Perry, D.C. (2003). Subtype-selective upregulation by chronic nicotine of high-affinity nicotinic receptors in rat brain demonstrated by receptor autoradiography. J. Pharmacol. Exp. Ther. *307*, 1090–1097.

Perry, D.C., Mao, D., Gold, A.B., McIntosh, J.M., Pezzullo, J.C., and Kellar, K.J. (2007). Chronic nicotine differentially regulates α6- and β3-containing nicotinic cholinergic receptors in rat brain. J. Pharmacol. Exp. Ther. *322*, 306–315.

Pomerleau, O.F., Downey, K.K., Stelson, F.W., and Pomerleau, C.S. (1995). Cigarette smoking in adult patients diagnosed with attention deficit hyperactivity disorder. J. Subst. Abuse *7*, 373–378.

Quik, M., and McIntosh, J.M. (2006). Striatal α6* nicotinic acetylcholine receptors: potential targets for Parkinson's disease therapy. J. Pharmacol. Exp. Ther. *316*, 481–489.

Revah, F., Bertrand, D., Galzi, J.L., Devillers-Thiery, A., Mulle, C., Hussy, N., Bertrand, S., Ballivet, M., and Changeux, J.P. (1991). Mutations in the channel domain alter desensitization of a neuronal nicotinic receptor. Nature *353*, 846–849.

Rice, M.E., and Cragg, S.J. (2004). Nicotine amplifies reward-related dopamine signals in striatum. Nat. Neurosci. *7*, 583–584.

Ritz, B., Ascherio, A., Checkoway, H., Marder, K.S., Nelson, L.M., Rocca, W.A., Ross, G.W., Strickland, D., Van Den Eeden, S.K., and Gorell, J. (2007). Pooled analysis of tobacco use and risk of Parkinson disease. Arch. Neurol. *64*, 990–997.

Salminen, O., Murphy, K.L., McIntosh, J.M., Drago, J., Marks, M.J., Collins, A.C., and Grady, S.R. (2004). Subunit composition and pharmacology of two classes of striatal presynaptic nicotinic acetylcholine receptors mediating dopamine release in mice. Mol. Pharmacol. *65*, 1526–1535.

Schultz, W. (2002). Getting formal with dopamine and reward. Neuron *36*, 241–263.

Shao, X.M., Tan, W., Xiu, J., Puskar, N., Fonck, C., Lester, H.A., and Feldman, J.L. (2008). α4* nicotinic receptors in preBotzinger complex mediate cholinergic/nicotinic modulation of respiratory rhythm. J. Neurosci. *28*, 519–528.

Tapper, A.R., McKinney, S.L., Nashmi, R., Schwarz, J., Deshpande, P., Labarca, C., Whiteaker, P., Marks, M.J., Collins, A.C., and Lester, H.A. (2004). Nicotine activation of α4* receptors: sufficient for reward, tolerance, and sensitization. Science *306*, 1029–1032.

Tapper, A.R., McKinney, S.L., Marks, M.J., and Lester, H.A. (2007). Nicotine responses in hypersensitive and knockout α4 mice account for tolerance to both hypothermia and locomotor suppression in wild-type mice. Physiol. Genomics *31*, 422–428.

Wathey, J.C., Nass, M.M., and Lester, H.A. (1979). Numerical reconstruction of the quantal event at nicotinic synapses. Biophys. J. *27*, 145–164.

Whiteaker, P., McIntosh, J.M., Luo, S., Collins, A.C., and Marks, M.J. (2000). [^{125}I]-α-Conotoxin MII identifies a novel nicotinic acetylcholine receptor population in mouse brain. Mol. Pharmacol. *57*, 913–925.

Wooltorton, J.R., Pidoplichko, V.I., Broide, R.S., and Dani, J.A. (2003). Differential desensitization and distribution of nicotinic acetylcholine receptor subtypes in midbrain dopamine areas. J. Neurosci. *23*, 3176–3185.

Zhang, H., and Sulzer, D. (2004). Frequency-dependent modulation of dopamine release by nicotine. Nat. Neurosci. *7*, 581–582.

Zhou, F.M., Liang, Y., and Dani, J.A. (2001). Endogenous nicotinic cholinergic activity regulates dopamine release in the striatum. Nat. Neurosci. *4*, 1224–1229.

Zhuang, X., Oosting, R.S., Jones, S.R., Gainetdinov, R.R., Miller, G.W., Caron, M.G., and Hen, R. (2001). Hyperactivity and impaired response habituation in hyperdopaminergic mice. Proc. Natl. Acad. Sci. USA *98*, 1982–1987.

Zoli, M., Moretti, M., Zanardi, A., McIntosh, J.M., Clementi, F., and Gotti, C. (2002). Identification of the nicotinic receptor subtypes expressed on dopaminergic terminals in the rat striatum. J. Neurosci. *22*, 8785–8789.

Neuron, Volume 60

Supplemental Data and Experimental Procedures

In Vivo Activation of Midbrain Dopamine Neurons via Sensitized, High-Affinity α6* Nicotinic Acetylcholine Receptors

Ryan M. Drenan, Sharon R. Grady, Paul Whiteaker, Tristan McClure-Begley, Sheri McKinney, Julie M. Miwa, Sujata Bupp, Nathaniel Heintz, J. Michael McIntosh, Merouane Bencherif, Michael J. Marks, and Henry A. Lester.

Supplementary Experimental Procedures

Materials

[^{3}H]-dopamine was obtained from Perkin Elmer (Boston, MA) (7,8-[^{3}H] at 30–50 Ci/mmol). Hepes, half sodium salt, was a product of Roche Applied Science (Indianapolis, IN). Ultra centrifugation grade sucrose was obtained from Fisher Chemicals (Fairlawn, NJ). Sigma-Aldrich (St. Louis, MO) was the source for the following compounds: L-(+)-arabinose, ascorbic acid, atropine sulfate, bovine serum albumin (BSA), (-)-nicotine tartrate, nomifensine, mecamylamine, R(+)-SCH23390, streptomycin, ampicillin, chloramphenicol, kanamycin, tetracycline, yohimbine, prazosin, and pargyline. Optiphase 'SuperMix' scintillation fluid was from Perkin Elmer Life Sciences.

Bacterial Artificial Chromosome Recombineering and Transgenesis

A bacterial artificial chromosome (BAC) RP24-149I12 containing the mouse α6 nicotinic receptor subunit gene (*Chrna6*) was obtained from the BACPAC Resource Center (BPRC) at Children's Hospital Oakland Research Institute (Oakland, CA). BAC recombineering was carried out using a Counter Selection BAC modification kit (Genebridges; Heidelberg, Germany). Recombineering in bacteria utilizes endogenous recombination activity, and allows the insertion of exogenous DNA into the BAC without residual sequences such as selection markers (neo) or loxP sites. α6 Leucine 280 (Leu9') was mutated to a serine using a two-step selection/counter selection protocol. First, a 15

bp stretch of α6 exon 5 (5'-gttctgctttctctc-3') containing the coding sequence for V278 through L282 was replaced with a cassette containing a tandem selection (neo)/counter selection (rpsL) marker. The rpsL/neo cassette was amplified by PCR using oligos designed to engineer α6 exon 5 homology arms flanking the sequence between and including V278 to L282. The oligo sequences were: forward primer: 5'-tt ttt tac ctt ccc tcc gac tgt ggc gag aaa gtg act ctt tgc atc tcc gcggccgc GGC CTG GTG ATG ATG GCG GGA TCG-3', and reverse primer: 5'-ac gag aga tgt gga tgg gat ggt ctc tgt aat cac cag caa aaa gac agt gcggccgc TCA GAA GAA CTC GTC AAG AAG GCG-3' (homology arms: lower case; *Not*I restriction site: underlined, lower case; rpsL/neo cassette priming sequence: upper case).

Neo was used to select positive recombinants, and an engineered *Not*I restriction site pair flanking the selection cassette was used to confirm the location of the exogenously inserted DNA within the BAC. In the second step, α6 exon 5 was restored using counter selection. Bacterial cells were placed under selective pressure (via streptomycin sensitivity gained by insertion of the rpsL marker) to lose the neo-rpsL cassette and replace it with non-selectable DNA engineered to insert the Leu9' to Ser (L280S) mutation. Non-selectable DNA sense strand sequence was: 5'-tt ttt tac ctt ccc tcc gac tgt ggc gag aaa gtg act ctt tgc atc tcc gtt ctg TCA agc ttg act gtc ttt ttg ctg gtg att aca gag acc atc cca tcc aca tct ctc gt-3' (L280S mutation in upper case, silent *Hind*III restriction site underlined). The resultant strain harbored a BAC with no ectopic DNA in or around the α6 gene. $\alpha6^{L9'S}$ BAC DNA was confirmed to have the desired mutation by DNA sequencing, restriction mapping, and diagnostic PCR. The α6 nicotinic receptor gene is directly adjacent to the β3 nicotinic receptor gene (*Chrnb3*). To eliminate the possibility that any physiological or behavioral phenotypes of our transgenic mice could be attributed to the presence of extra copies of β3, but to retain the β3 locus, we silenced the β3 gene using homologous recombination. β3 was silenced by replacing exon 1 (containing the methionine initiation codon) with an ampicillin selection cassette. An ampicillin marker derived from pCDNA3.1zeo was amplified by PCR using oligos designed to engineer β3 homology arms and diagnostic *Sbf*I restriction sites flanking the ampicillin marker. The oligo sequences were: forward primer: 5'-agc ctc aca aga cct gac agc tca ctg ggc atc agt gaa gtg cac cctgcagg GAC GTC AGG TGG CAC-3' and reverse

primer: 5'-tga gag agt ggc act gag agc caa gaa gac ccg tag gaa gcc tgt cctgcagg GTC TGA CGC TCA GTG-3' (homology arms: lower case; *Sbf*I restriction site: underlined, lower case; ampicillin marker priming sequence: upper case). Two additional genes (*4921537P18Rik* and *Tex24*) which are not expressed in brain are also contained on the final BAC construct.

Injection-grade $\alpha 6^{L9'S}$ BAC DNA was prepared via double CsCl banding (Lofstrand Labs; Gaithersberg, MD). To produce transgenic animals, BAC DNA was injected into the male pronucleus of recently fertilized FVB/N embryos and implanted into pseudopregnant Swiss-Webster surrogates. Transgenic founders were identified using tail biopsy DNA and PCR primers designed to detect both the L9'S mutation (forward: 5'-ctc cgt tct gtc aag ctt g-3', reverse: 5'-acg agt gct ctg aat tct ctg-3'), and the inserted ampicillin cassette within the β3 gene (forward: 5'-gct cat gag aca ata acc ctg-3', reverse: 5'-cag tct tgg aag caa cat cca gc-3'). Founders were crossed to C57BL/6J (Jackson Labs; Bar Harbor, ME) to obtain germline transmission and to establish a colony, and transgenic mice were continually backcrossed to C57BL/6J. Routine genotyping was done by multiplex PCR (forward primer #1: 5'-ctc cgt tct gtc aag ctt g-3', forward primer #2: 5'-ctg ctg ctc atc acc gag atc-3', reverse primer #1: 5'-acg agt gct ctg aat tct ctg-3', reverse primer #2: 5'-cag atg tca ccc aag atg ccg-3') analysis of tail DNA from newly weaned mice.

Mice

All experiments were conducted in accordance with the guidelines for care and use of animals provided by the National Institutes of Health, and protocols were approved by the Institutional Animal Care and Use Committee at the California Institute of Technology, the University of Colorado at Boulder, or the Rockefeller University. Mice were kept on a standard 12 h light/dark cycle at 22°C and given food and water *ad libitum*. On postnatal day 21, mice were weaned and housed with same-sex littermates. At 21 to 28 days, tail biopsies were taken for genotype analysis by PCR. Tails were digested in 50 mM NaOH at 95ºC for 45 minutes followed by neutralization with 0.5 M Tris-Cl, pH 5.5 and subsequent direct analysis by multiplex PCR. $\alpha 4^{L9'A}$ knock-in mice used in this study were generated on a mixed C57/129Sv background (1,2), and were

backcrossed at least 10 generations to C57BL/6. Wild type (WT) control mice were littermates of $\alpha6^{L9'S}$ transgenic mice.

Locomotor Activity

Mice used to study locomotion were eight to sixteen weeks old by the beginning of an experiment, and were back-crossed to C57BL/6 at least three times. Back-crossing to C57BL/6 did not affect locomotor activity. Mouse horizontal locomotor activity was measured with an infrared photobeam activity cage system (San Diego Instruments; San Diego, CA). Ambulation events were recorded when two contiguous photobeams were broken in succession. Acute locomotor activity in response to nicotinic ligands or other agents was studied by recording ambulation events during four 15 sec intervals per minute for a designated number of minutes. For most experiments, groups of eight mice were placed in the activity cages (18 X 28 cm) and their baseline level of activity was recorded for eight minutes. Mice were removed from their cage, injected (100 μl per 25 g body mass), and returned to the cage within 15 sec. For some experiments, mice were pre-injected with saline or an antagonist immediately prior to the start of the experiment, followed by challenge with nicotine eight minutes after the start of the experiment. For generation of locomotor activity concentration-response relationship profiles, a group of mice was administered saline and, after five to eight days off, each successive dose of drug. For experiments probing sensitization or tolerance, mice were injected once daily with saline for three days prior to the start of daily nicotine injections. For 48 h home cage monitoring, mice were isolated in their own cage and habituated to the test room and cage for 24 h. Following this, locomotor activity was recorded in 15 min intervals for 48 h.

Neurotransmitter Release from Striatal Synaptosomes

After a mouse was sacrificed by cervical dislocation, its brain was removed and placed immediately on an ice-cold platform and brain regions were dissected. Tissues from each mouse were homogenized in 0.5 ml of ice-cold 0.32 M sucrose buffered with 5 mM HEPES, pH 7.5. A crude synaptosomal pellet was prepared by centrifugation at 12,000 *g* for 20 min. The pellets were resuspended in “uptake buffer”: 128 mM NaCl, 2.4

mM KCl, 3.2 mM $CaCl_2$, 1.2 mM KH_2PO_4, 1.2 mM $MgSO_4$, 25 mM HEPES, pH 7.5, 10 mM glucose. For DA uptake, buffer was supplemented with 1 mM ascorbic acid and 0.01 mM pargyline, whereas for GABA uptake, buffer was supplemented with 1mM aminooxyacetic acid. For [^{3}H]GABA uptake, synaptosomes were incubated for 10 min at 37°C. [^{3}H]GABA and unlabeled GABA were then added to final concentrations of 0.1 and 0.25 μM, respectively, and the suspension was incubated for another 10 min. For DA uptake, synaptosomes were incubated at 37° C in uptake buffer for 10 min before addition of 100 nM [^{3}H]dopamine (1 μCi for every 0.2 ml of synaptosomes), and the suspension was incubated for an additional 5 min.

All experiments were conducted at room temperature using methods described previously (3,4) with modifications for collection into 96-well plates. In brief, aliquots of synaptosomes (80 μl) were distributed onto filters and perfused with buffer (uptake buffer containing 0.1% bovine serum albumin and 1 μM atropine with 1 μM nomifensine (for DA release) or 0.1 μM NNC-711 [1-(2-(((diphenylmethylene)amino)oxy)ethyl)-1,2,5,6-tetrahydro-3-pyridinecarboxylic acid hydrochloride]) (for GABA release) at 0.7 ml/min for 10 min, or buffer for 5 min followed by buffer with 50 nM αCtxMII. Aliquots of synaptosomes were then exposed to nicotine or high potassium (20 mM) in buffer for 20 sec to stimulate release of [^{3}H]dopamine or [^{3}H]GABA, followed by buffer. Fractions (~ 0.1 ml) were collected for 4 min into 96-well plates every 10 sec starting from 1 min before stimulation, using a Gilson FC204 fraction collector with a multicolumn adapter (Gilson, Inc.; Middleton, WI). Radioactivity was determined by scintillation counting using a 1450 MicroBeta Trilux scintillation counter (Perkin Elmer Life Sciences) after addition of 0.15 ml Optiphase 'SuperMix' scintillation cocktail. Instrument efficiency was 40 %.

Data were analyzed using SigmaPlot 5.0 for DOS. Perfusion data were plotted as counts per minute versus fraction number. Fractions collected before and after the peak were used to calculate baseline as a single exponential decay. The calculated baseline was subtracted from the experimental data. Fractions that exceeded baseline by 10 % or more were summed to give total released cpm and then normalized to baseline to give units of release [(cpm-baseline)/baseline] (3). Agonist dose response data were fit to the Hill equation (5).

Patch-Clamp Electrophysiology

For slice electrophysiology, transgenic and non-transgenic mice were identified by genotyping new litters at ~14 days after birth. Postnatal day 17-25 (for midbrain), 21-28 (for locus coeruleus), or 42-56 (for striatum) mice were anesthetized with sodium pentobarbital (40 mg/kg, i.p.) followed by cardiac perfusion with oxygenated (95% O_2/5% CO_2) ice-cold glycerol-based artificial CSF (gACSF) containing 252 mM glycerol, 1.6 mM KCl, 1.2 mM NaH_2PO_4, 1.2 mM $MgCl_2$, 2.4 mM $CaCl_2$, 18 mM $NaHCO_3$, and 11 mM glucose. Following perfusion, brains were removed and retained in gACSF (0–4°C). Coronal slices (midbrain, striatum: 250 μm; pons: 200 μm) were cut with a microslicer (DTK-1000; Ted Pella, Redding, CA) at a frequency setting of 9 and a speed setting of 3.25. Brain slices were allowed to recover for at least 1 h at 32°C in regular, oxygenated artificial CSF (ACSF) containing 126 mM NaCl, 1.6 mM KCl, 1.2 mM NaH_2PO_4, 1.2 mM $MgCl_2$, 2.4 mM $CaCl_2$, 18 mM $NaHCO_3$, and 11 mM glucose.

For recordings, a single slice was transferred to a 0.8 ml recording chamber (Warner Instruments, RC-27L bath with PH-6D heated platform). Slices were continually superfused with ACSF (1.5–2.0 ml/min) throughout the experiment. Cells were visualized with an upright microscope (BX 50WI; Olympus) and near-infrared illumination. Patch electrodes were constructed from Kwik-Fil borosilicate glass capillary tubes (1B150F-4; World Precision Instruments, Inc.; Sarasota, FL) using a programmable microelectrode puller (P-87; Sutter Instrument Co.; Novato, CA). The electrodes had tip resistances of 4.5–8.0 MΩ when filled with internal pipette solution (pH adjusted to 7.25 with Tris base, osmolarity adjusted to 290 mOsm with sucrose) containing: 135 mM potassium gluconate, 5 mM EGTA, 0.5 mM $CaCl_2$, 2 mM $MgCl_2$, 10 mM HEPES, 2 mM Mg-ATP, and 0.1 mM GTP.

Whole-cell recordings were taken at 32°C with an Axopatch 1D amplifier, a 16-bit Digidata 1322A A/D converter, and pCLAMP9.2 software (all Molecular Devices Axon; Sunnyvale, CA). Data were sampled at 5 kHz and low-pass filtered at 1 kHz. The junction potential between the patch pipette and the bath solution was nulled immediately prior to gigaseal formation. Series resistance was uncompensated. Putative GABAergic neurons in the SNr and DAergic neurons in SNc or VTA were identified according to

generally accepted criteria (4,6): (1) narrow spikes in GABA neurons vs. broad spikes in DA neurons; (2) rapid firing (> 10 Hz) in GABA neurons vs. slow firing (< 5 Hz) in DA neurons; (3) SNc DA neurons and to a lesser degree VTA DA neurons, but not SNr GABAergic neurons, express hyperpolarization-activated cation current (I_h). Noradrenergic neurons in locus coeruleus were identified by the following criteria: (1) expression of tyrosine hydroxylase as determined by immunohistochemistry; (2) pacemaker firing (≤ 2 Hz); (3) absence of I_h currents or significant adaptation of membrane potential in response to hyperpolarizing current injection; (4) location immediately medial to medial parabrachial nucleus. Striatal cholinergic interneurons were identified by the following criteria: 1) cholinergic cells are rare relative to medium spiny neurons, large (≥ 20 μm), and have 1-3 primary dendrites; 2) expression of I_h currents and significant membrane potential sag in response to hyperpolarizing current injection; 3) some cells do not fire spontaneously whereas other exhibit tonic, irregular firing (0-5 Hz).

To examine the function of somatic nAChRs, nicotine was locally applied using a Picospritzer II (General Valve; Fairfield, NJ). Using a piezoelectric translator (Burleigh Instruments; Fishers Park, NY), the pipette tip was moved within 20-40 μm of the recorded cell over a period of 250 ms starting 300 ms before drug application. Nicotine was then puffed at 10–20 psi for 250 ms. Fifty milliseconds after the application, the glass pipette was retracted over a period of 250 ms.

Real Time PCR

Mouse genomic DNA was obtained from tail biopsies. Relative quantification of total α6 gene copies was performed using the LightCycler 480 system and SYBR Green I Master Mix (Roche Diagnostics; Indianapolis, IN). The α6 (WT and L9'S alleles) locus was detected with an α6-specific primer set (forward primer: 5'-gag cgc tgc tga cac ttg-3', reverse primer: 5'-ccc ctt gta gca cct agc-3'). The α4 nicotinic receptor genomic locus, which is assumed to be present at one copy per haploid genome, was used as a reference target and was detected with α4-specific primers (forward primer: 5'-ctg ctg ctc atc acc gag atc-3', reverse primer: 5'-cag atg tca ccc aag atg ccg-3'). Crossing point values were obtained for target (α6) and reference (α4) genes in serial dilutions of gDNA

from non-transgenic and transgenic mice. The relative ratio of α6 genomic copies in non-transgenic versus transgenic mice was calculated according to accepted standards (7).

RT-PCR

For RNA analysis, mice were anesthetized with halothane and sacrificed by cervical dislocation. Brains were rapidly removed and extracted in ice-cold Trizol (Invitrogen; Carlsbad, CA) (1 ml Trizol per 100 mg wet brain tissue) aided by dounce homogenization. RNA was purified according to the manufacturer's instructions, resuspended in DEPC-treated H_20, and stored at -80ºC. RNA quality was assessed by observing absorbance profiles across a range of wavelengths between 220 nm and 320 nm. Spectrophotometric analysis was performed using a ND-1000 spectrophotometer (NanoDrop; Wilmington, DE). Reverse transcription and target amplification was performed using SuperScript III One-Step RT-PCR enzyme mix (Invitrogen). Gene-specific primers for total α6 mRNA (mutant and WT; forward primer: 5'-gtt tta cac cat caa cct cat c-3', reverse primer: 5'-tta gga gtc tgt gta ctt ggc-3') or $\alpha6^{L9'S}$ mRNA (forward primer: 5'-ctc cgt tct gtc aag ctt g-3', reverse primer: 5'-acg agt gct ctg aat tct ctg-3') were used to prime first-strand cDNA synthesis and subsequent double-stranded PCR product. In control reactions, *Taq* DNA polymerase was substituted for SuperScript III enzyme mix.

$^{86}Rb^+$ Efflux from Superior Colliculus Synaptosomes

Nicotine-stimulated $^{86}Rb^+$ efflux from superior colliculus (SC) was measured as described previously(8). SC was dissected from adult mice sedated with halothane and sacrificed by cervical dislocation. Tissue was homogenized by hand in 1 ml of ice-cold 0.32 M sucrose buffered to pH 7.5 with HEPES using a glass/Teflon tissue grinder. After homogenization, the grinder was rinsed three times with 0.5 ml of buffered sucrose solution. A crude synaptosomal pellet was obtained by centrifugation at 12,000 *g* for 20 min. After removal of the sucrose, each pellet was resuspended in load buffer (140 mM NaCl, 1.5 mM KCl, 2 mM $CaCl_2$, 1 mM $MgSO_4$, 25 mM HEPES, and 22 mM glucose) and placed on ice until incubation with $^{86}RbCl$. SC synaptosomes were incubated with 4

μCi of $^{86}Rb^{+}$ for 30 min in a final volume of 35 μl of load buffer, after which samples were collected by gentle filtration onto a 6-mm-diameter Gelman-type A/E glass filter and washed once with 0.5 ml of load buffer. Filters containing the synaptosomes loaded with $^{86}Rb^{+}$ were transferred to a polypropylene platform and superfused for 5 min with effluent buffer (135 mM NaCl, 1.5 mM KCl, 5 mM CsCl, 2 mM $CaCl_2$, 1 mM $MgSO_4$, 25 mM HEPES, 22 mM glucose, 50 nM tetrodotoxin, and 0.1% bovine serum albumin). A peristaltic pump applied buffer to the top of the synaptosome containing filter at a rate of 2 ml/min, and a second peristaltic pump set at a faster flow rate of 3 ml/min removed buffer from the bottom of the platform. The greater speed of the second pump prevented pooling of buffer on the filter. Effluent buffer was pumped through a 200 μl Cherenkov cell and into a β-Ram detector (IN/US Systems; Tampa, FL). Radioactivity was measured for 3 min with a 3 s detection window providing 60 data points for each superfusion. Each aliquot was stimulated by 1 of 4 different nicotine concentrations, with a 5 s exposure for each concentration.

[^{125}I]-α-conotoxin MII Binding to Brain Sections

Two mice for each genotype (WT, $\alpha6^{L9'S}$ line 2 and 5) were sedated with halothane and sacrificed by cervical dislocation. The brains were removed and rapidly frozen by immersion in isopentane (-35°C, 60 s). The frozen brains were wrapped in aluminum foil, packed in ice, and stored at -70°C until sectioning. Tissue sections (14 μm) prepared using an IEC Minotome Cryostat refrigerated to -16°C were thaw mounted onto Fisher Superfrost/Plus Microscope Slides. Mounted sections were stored desiccated at -70°C until use. Eight series of sections were collected from each mouse brain.

Before incubation with [^{125}I]-αCtxMII, three adjacent series of sections from each mouse were incubated in binding buffer (144 mM NaCl, 1.5 mM KCl, 2 mM $CaCl_2$, 1 mM $MgSO_4$, 20 mM HEPES, 0.1% BSA (w/v), pH 7.5) containing 1 mM phenylmethylsulfonyl fluoride at 22°C for 15 min. For all [^{125}I]-αCtxMII binding reactions, the standard binding buffer was supplemented with BSA [0.1% (w/v)], 5 mM EDTA, 5 mM EGTA, and 10 mg/ml each of aprotinin, leupeptin trifluoroacetate, and pepstatin A to protect the ligand from endogenous proteases. The sections were then incubated with 0.5 nM [^{125}I]-αCtxMII for 2 h at 22°C. Samples were washed as follows:

once for 30 sec in binding buffer plus 0.1% BSA at 22ºC, twice for 30 sec in binding buffer plus 0.1% BSA (4ºC), twice for 5 sec in 0.1X binding buffer plus 0.01% BSA (4ºC) and twice for 5 sec in 5 mM HEPES, pH 7.5 (0ºC). Sections were initially dried with a stream of air, then by overnight storage (22°C) under vacuum. Mounted, desiccated sections were apposed to film (1–3 days, Kodak MR film).

[^{125}I]-Epibatidine Binding to Membranes

Each mouse was sacrificed by cervical dislocation. The brain was removed and placed on an ice-cold platform. Tissue was collected from superior colliculus, thalamus, striatum (CPu and dorsal NAc), and olfactory tubercle, then homogenized in ice-cold hypotonic buffer (144 mM NaCl; 0.2 mM KCl; 0.2 mM $CaCl_2$; 0.1 mM $MgSO_4$; 2 mM HEPES; pH 7.5) using a glass-Teflon tissue grinder(9). Particulate fractions were obtained by centrifugation at 20,000 g (15 min, 4ºC; Sorval RC-2B centrifuge). The pellets were resuspended in fresh homogenization buffer, incubated at 22ºC for 10 min, then harvested by centrifugation as before. Each pellet was washed twice more by resuspension/centrifugation, then stored (in pellet form under homo-genization buffer) at -70ºC until use. Protein was quantified with a Lowry assay using bovine serum albumin as the standard.

Binding of [^{125}I]-epibatidine was quantified using a modified version of the methods previously described for [^{3}H]-epibatidine (9). Incubations were per-formed in 96-well polystyrene plates, in 30 ml of binding buffer (144 mM NaCl; 1.5 mM KCl; 2 mM $CaCl_2$; 1 mM $MgSO_4$; 20 mM HEPES; pH 7.5). Plates were covered to minimize evaporation during incubation, and all incubations progressed for 2 h at 22ºC. Saturation binding experiments were performed for membrane preparations from each brain region, using a [^{125}I]-epibatidine ligand concentration of 200 pM. Binding reactions were terminated by filtration of samples onto a single thickness of polyethyleneimine-soaked (0.5% w/v in binding buffer) GFA/E glass fiber filters (Gelman Sciences; Ann Arbor, MI) using an Inotech Cell Harvester (Inotech; Rockville, MD, U.S.A.). Samples were subsequently washed six times with ice-cold binding buffer. Bound ligand was quantified by gamma counting at 83-85% efficiency, using a Packard Cobra counter. In experiments with competitive, unlabeled αCtxMII, the amount of membrane protein added was

chosen to produce maximum binding of ligand to the tissue of approximately 40 Bq/well (less than 10% of total ligand added, minimizing the effects of ligand depletion). For αCtxMII (50 nM), the medium was supplemented with bovine serum albumin (0.1% w/v) as a carrier protein. For all experiments, non-specific binding was determined in the presence of 1 mM (-)-nicotine tartrate.

Immunohistochemistry and Spectral Confocal Imaging

Coronal brain slices cut for patch-clamp recording were removed from the recording chamber and immediately fixed (4% PFA in PBS, pH 7.4) for 45 min at 4ºC. Slices were permeabilized (20 mM Hepes, pH 7.4, 0.5% Triton X-100, 50 mM NaCl, 3 mM $MgCl_2$, 300 mM sucrose) for 1 h at 4ºC followed by blocking (0.1% Triton X-100, 5% donkey serum in TBS) for 1 h at room temperature. Slices were incubated overnight at 4ºC in rabbit anti-tyrosine hydroxylase (TH) primary antibody (Pel-Freez; Rogers, AR) (diluted 1:100 in 0.1% Triton X-100, 5% donkey serum in TBS), washed three times in TBST (0.1% Triton X-100 in TBS), incubated for 1 h at room temperature in goat anti-rabbit Alexa 488 secondary antibody (Molecular Probes; Eugene, OR) (diluted 1:500 in 0.1% Triton X-100, 5% donkey serum in TBS), and washed three times in TBST.

Slices were mounted and imaged with a Nikon (Nikon Instruments, Melville, NY) C1 laser-scanning confocal microscope system equipped with spectral imaging capabilities and a Prior (Rockland, ME) remote-focus device. A Nikon Plan Apo 10X objective was used, and pinhole diameter was 30 μm. Sections were imaged at 12-bit intensity resolution over 512 X 512 pixels at a pixel dwell time of 6 μs. Alexa 488 was excited with an argon laser at 488 nm. Imaging was carried out using the Nikon C1si DEES grating and spectral detector with 32 parallel photomultiplier tubes. Signal from Alexa 488 was unmixed from background autofluorescence similar to our previous studies (4,10,11).

Statistics and Data Analysis

Physiology, neurochemistry, and real time PCR data are reported as mean $\pm$ SEM. Statistical significance ($p < 0.05$) was determined with a *t* test for continuous data meeting parametric assumptions for normality and equal variance. DA release

parameters and behavior data were analyzed for significance with two-way or one-way ANOVA, respectively, with Tukey post hoc analysis.

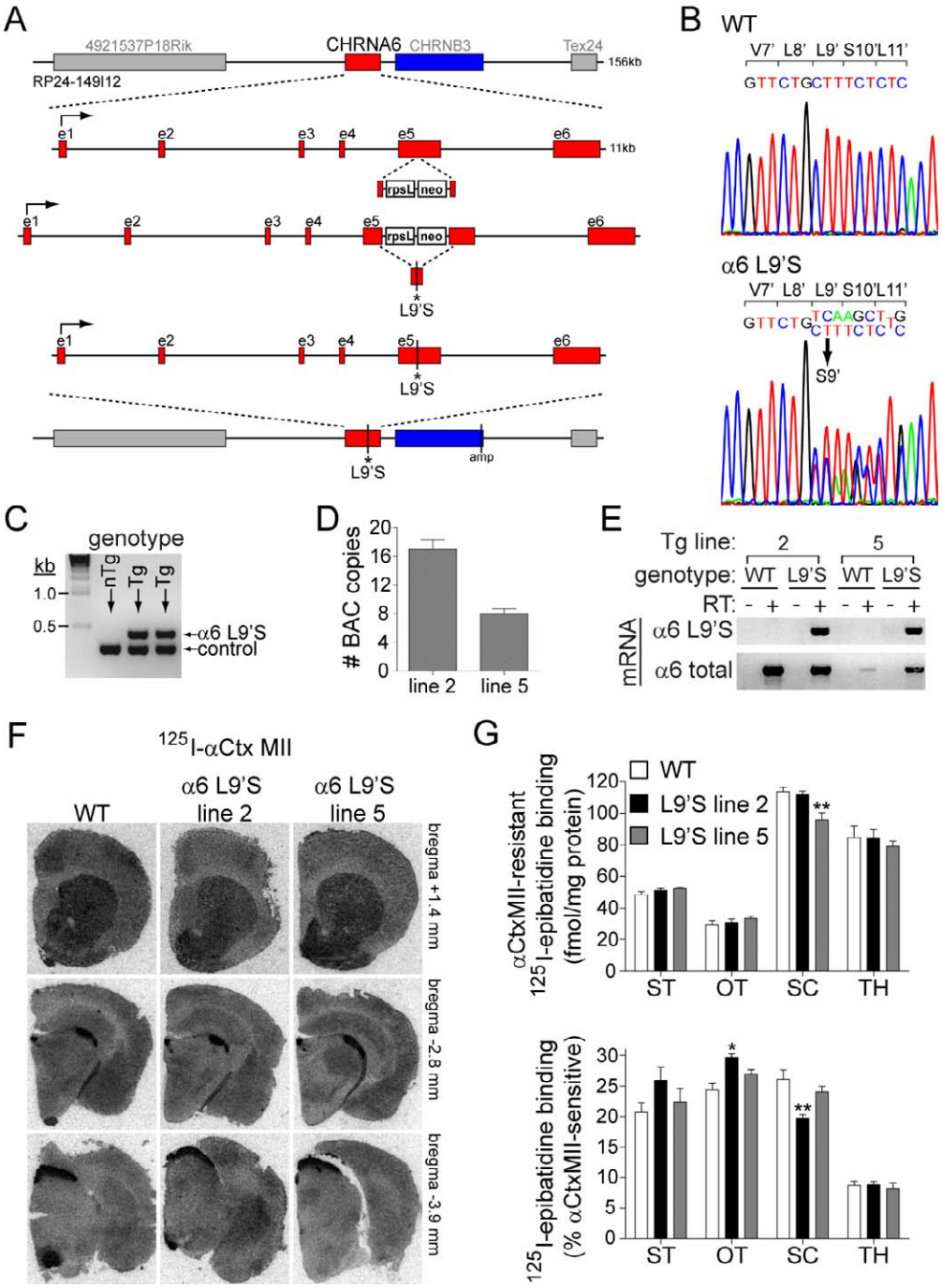

Figure S1 - Construction of α6 Leu9'Ser BAC transgenic mice.

(A) BAC recombineering to generate $\alpha6^{L9'S}$ targeting vector. Mouse BAC clone RP24-149I12 contains 156 kb of mouse genomic DNA, including the α6 (*Chrna6*) and β3 (*Chrnb3*) nicotinic receptor genes. A two-step homologous recombination procedure was carried out in *E. coli* to generate the $\alpha6^{L9'S}$ allele. First, a region of α6 exon 5 containing the Leu9' residue was replaced with an rpsL-neo selection cassette. Second, non-

selectable DNA containing the mutant Leu9'Ser sequence was inserted into exon 5 via counter-selection. The resulting BAC had no ectopic DNA sequences and differed from the WT α6 gene only at the Leu9' residue. The β3 nAChR gene on this BAC was inactivated by disruption of the start codon with an ampicillin cassette.

(B) Genomic DNA sequence of WT and transgenic mice demonstrate the presence of WT and Leu9'Ser α6 alleles in transgenic mice, and only WT α6 alleles in non-transgenic mice.

(C) Analysis of genomic DNA samples to identify non-transgenic and transgenic mice. Primers designed to amplify control (α4 nAChR) and $\alpha6^{L9'S}$ genomic DNA were used in multiplex PCR reactions to genotype weanling mice.

(D) Transgene copy number analysis. Real time quantitative PCR analysis on genomic DNA was used to quantify the number of $\alpha6^{L9'S}$ BAC transgenes in two independently derived transgenic lines (line 2 and line 5).

(E) Characterization of α6 (WT and L9'S) mRNA expression in line 2 and 5 with RT-PCR. Whole-brain RNA samples from non-transgenic and transgenic mice were reverse-transcribed and amplified with primers specific for total or L9'S α6 cDNA.

(F) Correct regional expression of α6* receptors in $\alpha6^{L9'S}$ mice. Brains from WT and $\alpha6^{L9'S}$ mice were sectioned and labeled with [^{125}I]-αCtxMII. Representative sections through striatum (bregma +1.4 mm), optic tract / hippocampus (bregma -2.8 mm), and superior colliculus (bregma -3.9 mm) are shown.

(G) Quantitative analysis of α6* receptor expression. Brain regions known to express α6* receptors were dissected and labeled with [^{125}I]-epibatidine in the presence or absence of competing, unlabeled αCtxMII. Raw binding values for αCtxMII-resistant receptors are shown in the upper panel. αCtxMII-sensitive receptors (predominantly α6*) are expressed as the percent of total epibatidine binding. ST, striatum; OT, olfactory tubercle; SC, superior colliculus; TH, thalamus.

Data are reported as mean $\pm$ SEM. *, $p < 0.05$; **, $p < 0.01$.

DA Release Parameters

	Nicotine (ST)	WT	L9'S line 2	L9'S line 5
Total	EC50 (±SEM)	0.36 ± 0.07	0.12 ± 0.02	0.17 ± 0.04
	Rmax (±SEM)	20.9 ± 1.0	21.4 ± 0.9	20.8 ± 1.2
MII-sensitive	EC50 (±SEM)	0.11 ± 0.04	0.047 ± 0.011	0.044 ± 0.011
	Rmax (±SEM)	5.41 ± 0.54	12.4 ± 0.6	9.56 ± 0.60
MII-resistant	EC50 (±SEM)	0.56 ± 0.12	0.47 ± 0.08	0.64 ± 0.11
	Rmax (±SEM)	15.6 ± 1.00	8.79 ± 0.43	11.4 ± 0.5
20 mM K^+		13.75 ± 0.24	10.76 ± 0.49	10.68 ± 0.43

	Nicotine (OT)	WT	L9'S line 2	L9'S line 5
Total	EC50 (±SEM)	0.31 ± 0.07	0.043 ± 0.006	0.064 ± 0.013
	Rmax (±SEM)	33.1 ± 2.1	36.0 ± 1.3	34.3 ± 1.7
MII-sensitive	EC50 (±SEM)	0.082 ± 0.037	0.025 ± 0.004	0.029 ± 0.008
	Rmax (±SEM)	7.03 ± 0.86	23.5 ± 1.0	19.7 ± 1.2
MII-resistant	EC50 (±SEM)	0.35 ± 0.10	0.40 ± 0.07	0.42 ± 0.14
	Rmax (±SEM)	23.7 ± 2.0	17.1 ± 0.9	17.0 ± 1.7
20 mM K^+		16.62 ± 0.96	14.43 ± 1.16	14.62 ± 1.31

Figure S2 – Dopamine release parameters for nicotine. WT, $\alpha6^{L9'S}$ line 2 and $\alpha6^{L9'S}$ line 5 striata were dissected and prepared for [^{3}H]DA release as described in Experimental Procedures. Striatum (ST) and olfactory tubercle (OT) were handled separately. Concentration-response data were fitted to the Hill equation. EC_{50} and R_{max} values are shown for each condition. Parallel samples were stimulated with KCl (20 mM) as a positive control. EC_{50} values are in μM. 20 mM K^+ and R_{max} values are in DA release units.

GABA Release Parameters

	Nicotine (ST/OT)	WT	L9'S line 2	L9'S line 5
Total	EC50 (±SEM)	1.30 ± 0.32	1.53 ± 0.44	2.47 ± 0.81
	Rmax (±SEM)	1.64 ± 0.32	1.25 ± 0.06	1.22 ± 0.11
MII-sensitive	EC50 (±SEM)	no activity	no activity	no activity
	Rmax (±SEM)	no activity	no activity	no activity
MII-resistant	EC50 (±SEM)	1.50 ± 0.47	4.18 ± 2.54	2.00 ± 0.54
	Rmax (±SEM)	1.40 ± 0.08	1.26 ± 0.08	1.30 ± 0.10
20 mM K^+		8.31 ± 0.34	8.24 ± 0.45	8.43 ± 0.50

Figure S3 – GABA release parameters for nicotine. WT, $\alpha6^{L9'S}$ line 2 and $\alpha6^{L9'S}$ line 5 striata were dissected and prepared for [^{3}H]DA release as described in Experimental Procedures. Striatum (ST) and olfactory tubercle (OT) were combined. Concentration-response data were fitted to the Hill equation. EC_{50} and R_{max} values are shown for each condition. MII-sensitive activity could not be fit and EC_{50} and R_{max} values could not be derived. Parallel samples were stimulated with KCl (20 mM) as a positive control. EC_{50} values are in μM. 20 mM K^+ and R_{max} values are in DA release units.

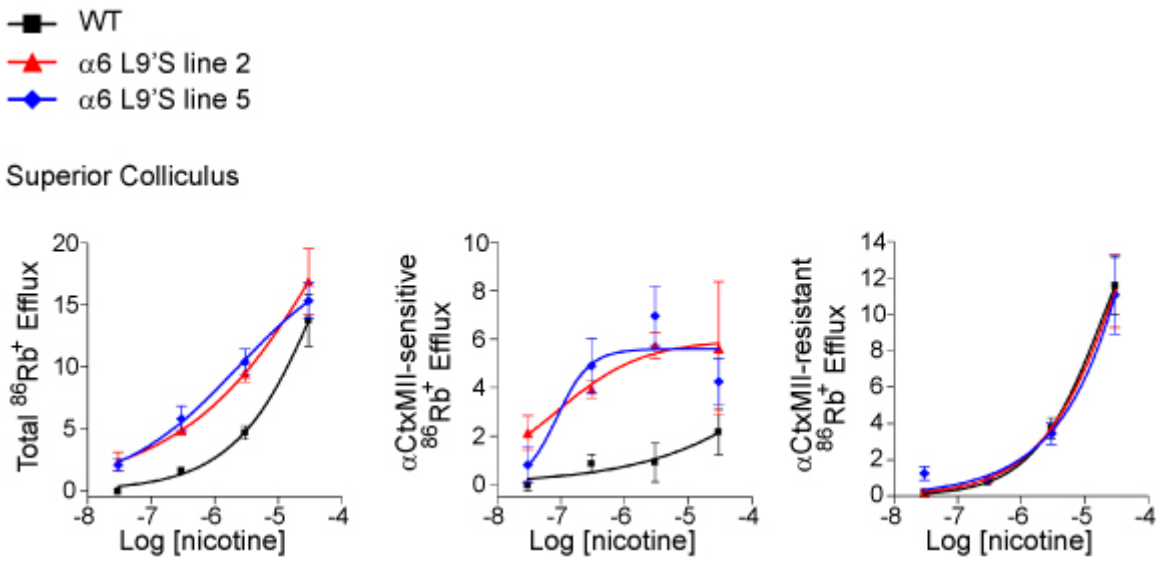

Figure S4 - Hypersensitive α6* receptors in superior colliculus of $\alpha6^{L9'S}$ mice. Superior colliculi from WT and $\alpha6^{L9'S}$ (line 2 and 5) were dissected and a crude synaptosomal pellet was prepared. Following $^{86}Rb^{+}$ loading, samples were stimulated with a range of nicotine concentrations and $^{86}Rb^{+}$ efflux was measured. Data were fitted to the Hill equation, and a concentration response curve for each mouse line (n = 6) is shown for total $^{86}Rb^{+}$ efflux (left panel). To determine the relative contribution of α6* and non-α6* receptors to the total efflux profile, parallel samples were incubated with αCtxMII (50 nM). αCtxMII-sensitive (center panel) and resistant (right panel) components are shown for each mouse line.

DA Release Parameters

	TC 2429 (ST/OT)	WT	L9'S line 2	L9'S line 5
Total	EC50 (±SEM)	0.0093 ± 0.005	0.0022 ± 0.0003	0.0026 ± 0.0004
	Rmax (±SEM)	8.68 ± 1.25	12.87 ± 0.37	11.86 ± 0.41
	10 μM nic	17.70	17.30	16.70
	% 10 μM nic	49.0	73.40	71.00
MII-sensitive	EC50 (±SEM)	0.0058 ± 0.0035	0.0016 ± 0.00014	0.0019 ± 0.0003
	Rmax (±SEM)	4.29 ± 0.44	10.4 ± 0.14	9.11± 0.25
	10 μM nic	3.19	8.53	5.97
	% 10 μM nic	134.60	122.00	152.70
MII-resistant	EC50 (±SEM)	0.014 ± 0.006	0.01 ± 0.003	0.011 ± 0.0039
	Rmax (±SEM)	4.39 ± 0.32	2.64 ± 0.14	3.07± 0.19
	10 μM nic	14.55	8.75	10.78
	% 10 μM nic	30.24	30.17	28.48

	TC 2403 (ST/OT)	WT	L9'S line 2	L9'S line 5
Total	EC50 (±SEM)	2.36 ± 0.56	0.70 ± 0.15	0.82 ± 0.22
	Rmax (±SEM)	12.37 ± 0.93	10.72 ± 0.61	10.57 ± 0.74
	10 μM nic	16.69	19.68	20.65
	% 10 μM nic	74.11	54.47	51.19
MII-sensitive	EC50 (±SEM)	0.06 ± 0.18	0.19 ± 0.04	0.1 ± 0.063
	Rmax (±SEM)	0.47 ± 0.2	4.83 ± 0.15	3.43 ± 0.32
	10 μM nic	1.63	10.77	10.39
	% 10 μM nic	28.83	44.85	33.01
MII-resistant	EC50 (±SEM)	2.85 ± 0.35	3.53 ± 0.83	4.03 ± 0.84
	Rmax (±SEM)	12.32 ± 0.26	7.26 ± 0.29	9.3 ± 0.33
	10 μM nic	15.07	8.91	10.26
	% 10 μM nic	81.78	81.48	90.64

Figure S5 – Dopamine release parameters for TC 2429 and TC 2403. WT, $\alpha6^{L9'S}$ line 2 and $\alpha6^{L9'S}$ line 5 striata were dissected and prepared for [^{3}H]DA release as described in Experimental Procedures. Striatum (ST) and olfactory tubercle (OT) were combined. Concentration-response data were fitted to the Hill equation. EC_{50} and R_{max} values are shown for each condition. Parallel samples were stimulated with nicotine (10 μM) as a positive control and to demonstrate partial or full agonism. EC_{50} values are in μM. 10 μM nicotine and R_{max} values are in DA release units.

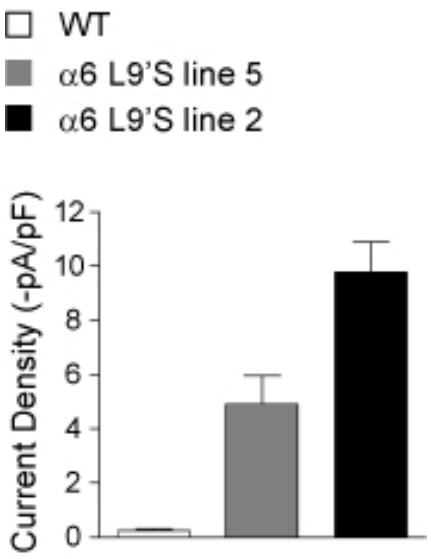

Figure S6 - Nicotinic current density in WT and $\alpha6^{L9'S}$ VTA neurons. VTA neurons from WT or $\alpha6^{L9'S}$ (line 2 and 5) were locally stimulated with nicotine (1 μM). Current responses (pA) were normalized to cell capacitance (pF) values for each cell.

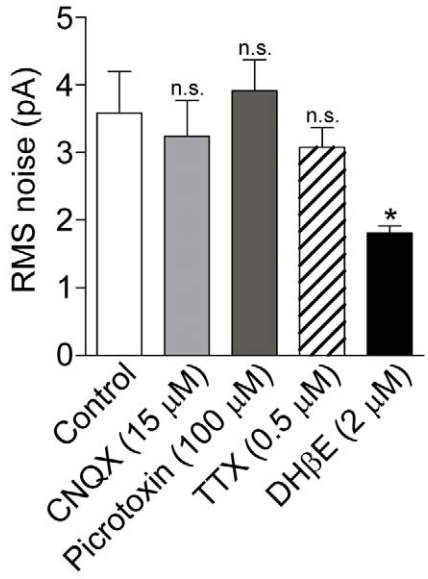

Figure S7 – Additional analysis of increased channel noise in VTA of $\alpha6^{L9'S}$ mice. Average RMS noise values for voltage clamp recordings from $\alpha6^{L9'S}$ VTA DA neurons under control conditions and in the presence of the indicated drug is shown. Because results were similar in line 2 and line 5, data from both lines were pooled.
Data are reported as mean $\pm$ SEM. n.s., not significant; *, $p < 0.05$.

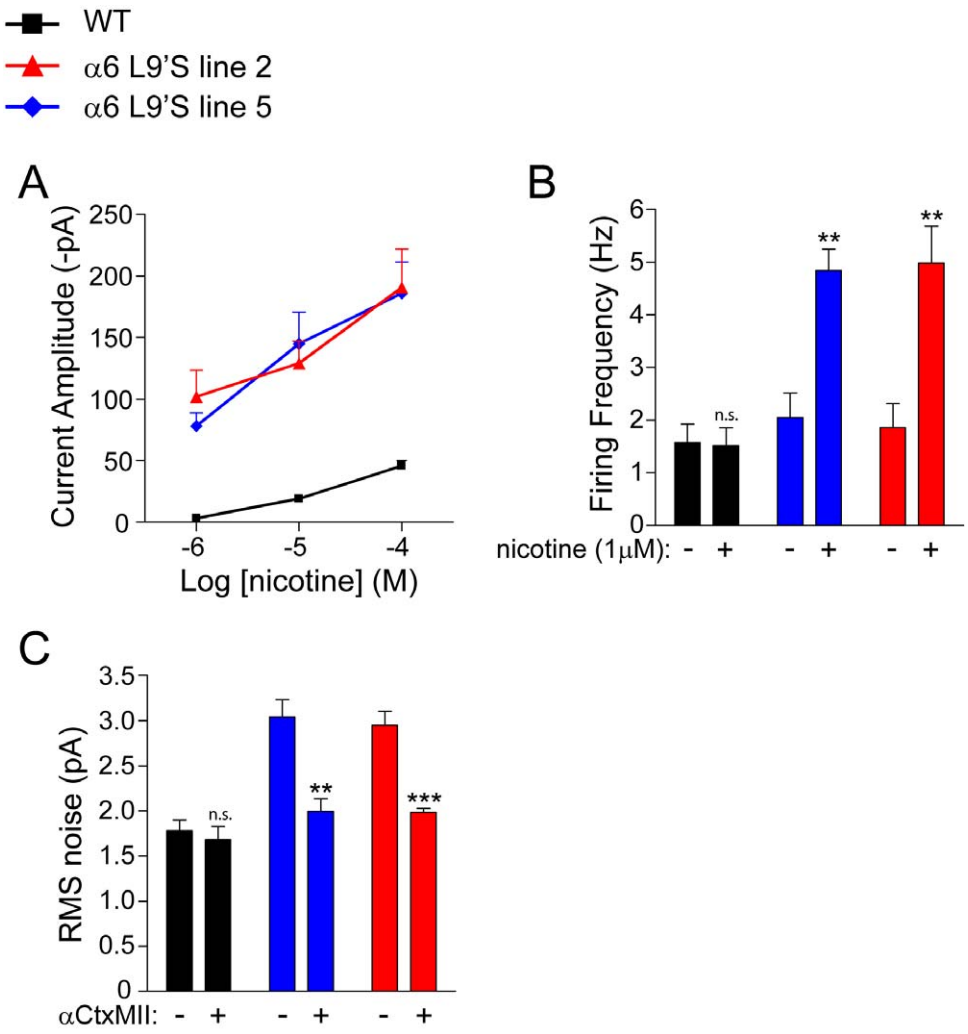

Figure S8 – Electrophysiological analysis of substantia nigra pars compacta (SNc) neurons.

(A) Concentration-response relationship for hypersensitive nicotinic responses in SNc neurons from WT and $\alpha6^{L9'S}$ mouse lines. The average peak amplitude of the cellular response for each mouse line and each nicotine concentration is plotted.

(B) Quantification of firing responses in WT and $\alpha6^{L9'S}$ SNc DA neurons. Peak instantaneous firing frequency values for each nicotine (1 μM) application (one per cell) were derived and averaged for each mouse line. Average peak values are compared with the average baseline firing rate for the same group of cells.

(C) Quantification of channel noise increase in $\alpha6^{L9'S}$ mice. RMS noise values for voltage clamp recordings from SNc DA neurons in the presence and absence of αCtxMII is shown.

Data are reported as mean $\pm$ SEM. n.s., not significant; **, $p < 0.01$; ***, $p < 0.001$. .

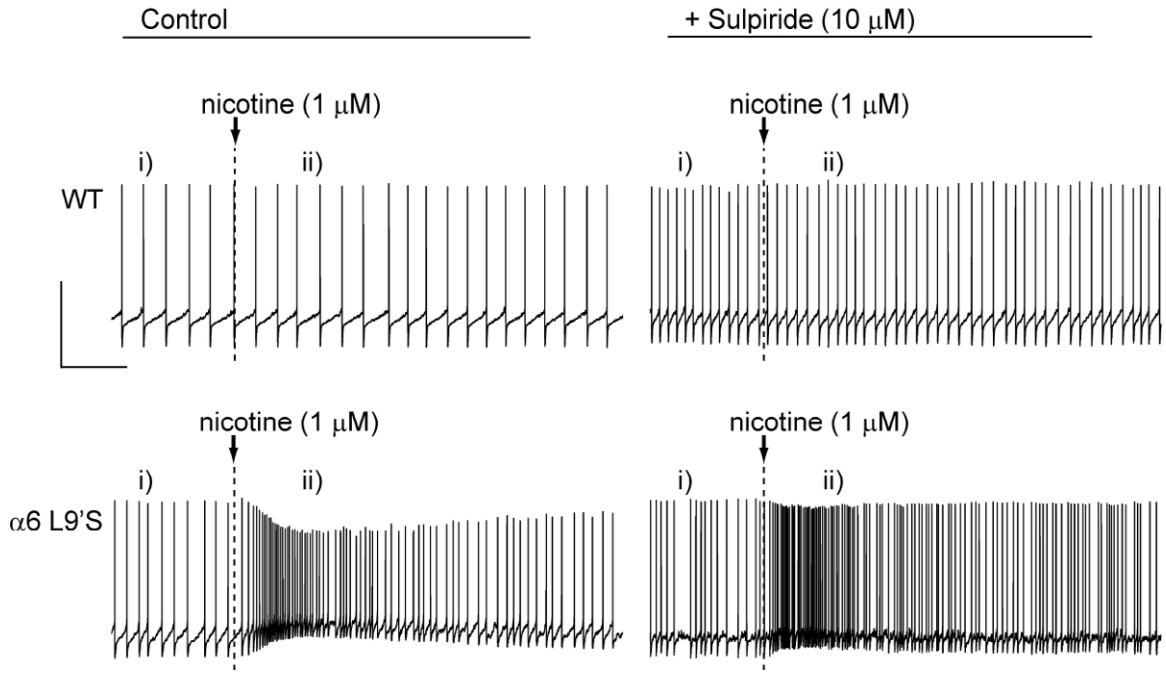

Figure S9 – Equivalent dopamine tone in WT and $\alpha6^{L9'S}$ VTA. VTA dopamine neurons from WT (top panel) or $\alpha6^{L9'S}$ (bottom panel) mice were recorded in whole-cell configuration. Baseline firing (control) and firing during bath application of sulpiride (10 μM) was recorded (i). Nicotine (1 μM) was puff applied (arrow; (ii)) both under baseline firing conditions and after 5 min of sulpiride application. Results were similar in line 2 (n = 2) and line 5 (n = 3). Representative traces are shown. Scale bars: 70 mV, 2.5 s.

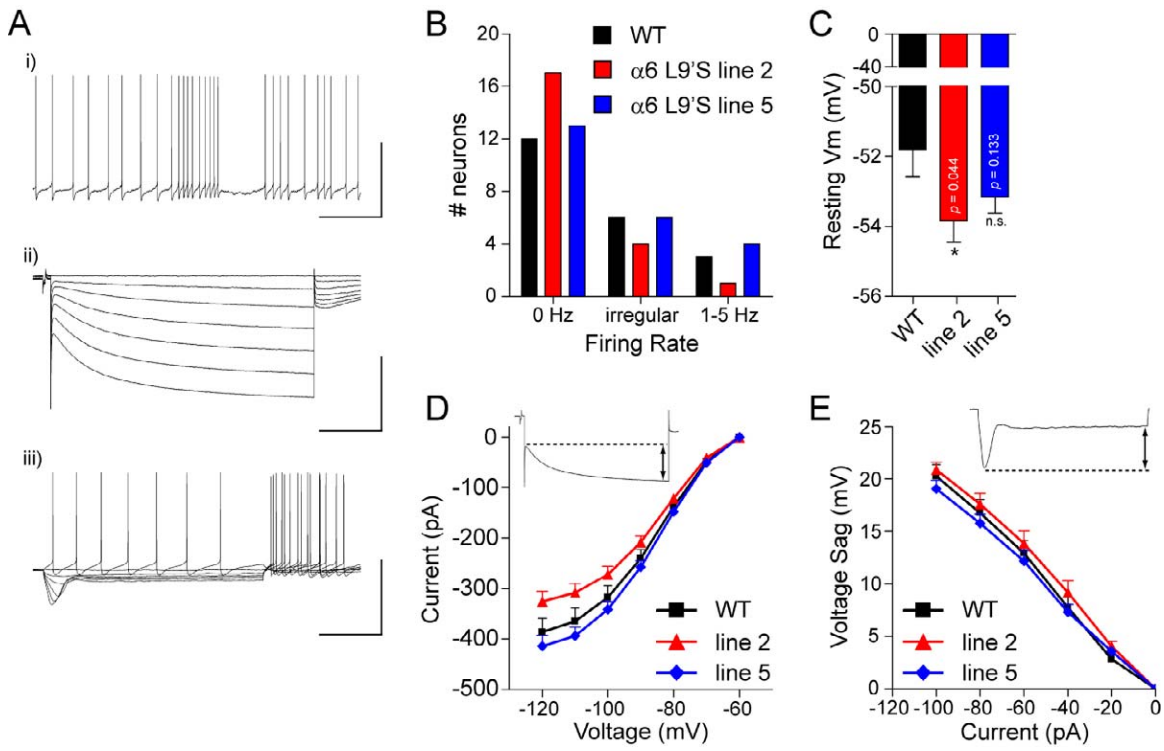

Figure S10 – Analysis of striatal cholinergic interneurons from WT and $\alpha6^{L9'S}$ mice.

(A) Identification of striatal cholinergic interneurons. Large, aspiny neurons from dorsal striatum often fired spontaneously (i; scale bars: 80 mV, 4 s) but in an irregular fashion, with periods of regular firing, bursts, and pauses in firing accompanied with a hyperpolarization in the resting membrane potential. Cholinergic cells expressed prominent I_h (ii; 400 pA, 0.4 s; Vm stepped from -60 mV to -70, -80, -90, -100, -110, and -120) and exhibited a substantial sag in the membrane potential in response to hyperpolarizing current pulses (iii; scale bars: 80 mV, 0.4 s; current (pA) pulses: +20, 0, -20, -40, -60, -80, -100).

(B) Spontaneous firing properties of WT and $\alpha6^{L9'S}$ cholinergic interneurons. Cells from the indicated group (WT, n = 21; line 2, n = 22; or line 5, n = 23) were classified as not firing (0 Hz), irregular firing, or regular firing (1-5 Hz).

(C) Resting membrane potential in WT and $\alpha6^{L9'S}$ cholinergic interneurons is plotted. n.s., not significant; *, $p < 0.05$.

(D) I_h in cholinergic interneurons is largely unchanged in $\alpha6^{L9'S}$ mice. Striatal cholinergic interneurons from WT, line 2, and line 5 were recorded in whole-cell configuration at a holding potential of -60 mV. Membrane voltage was stepped to the

indicated hyperpolarized potential, and hyperpolarization-activated currents were measured. These currents were defined as the difference between the steady-state current and the initial current level after the capacitive transient (inset).

(E) Hyperpolarizing current-induced voltage sag is unchanged in $\alpha6^{L9'S}$ mice. Striatal cholinergic interneurons from WT, line 2, and line 5 were recorded in whole-cell configuration in current clamp mode. Membrane potential, including the sag in the membrane potential that is dependent on I_h, was measured in response to the indicated hyperpolarizing current injections. Voltage sag for each current injection was defined as the difference between the peak hyperpolarized potential and the steady state potential at the end of the current pulse (inset).

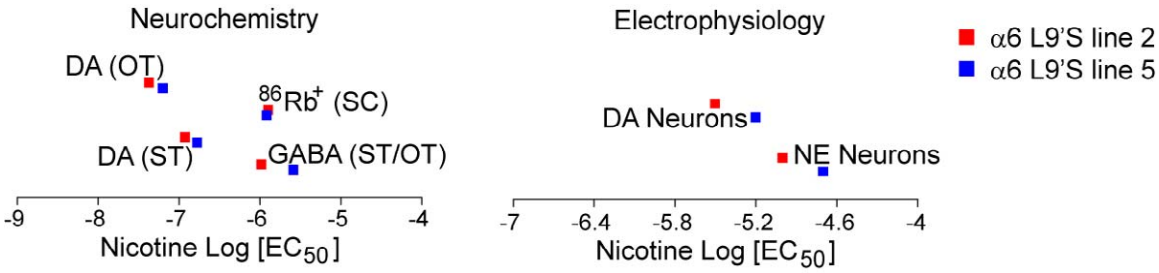

Figure S11 - Summary of nicotine EC_{50} values for functional nAChRs in $\alpha6^{L9'S}$ mice demonstrates DA neuron hypersensitivity. For neurochemistry experiments (left panel; [^{3}H]DA release, [^{3}H]GABA release, and $^{86}Rb^+$ efflux), nicotine EC_{50} values are plotted for $\alpha6^{L9'S}$ line 2 and 5. For slice electrophysiology (right panel), approximate EC_{50} values for picospritzer-activated currents are plotted for $\alpha6^{L9'S}$ VTA DA and LC NE neurons. OT, olfactory tubercle; ST, striatum; SC, superior colliculus.

Supplementary References

1. Fonck, C., Cohen, B. N., Nashmi, R., Whiteaker, P., Wagenaar, D. A., Rodrigues-Pinguet, N., Deshpande, P., McKinney, S., Kwoh, S., Munoz, J., Labarca, C., Collins, A. C., Marks, M. J., and Lester, H. A. (2005) *J Neurosci* **25**(49), 11396-11411
2. Tapper, A. R., McKinney, S. L., Nashmi, R., Schwarz, J., Deshpande, P., Labarca, C., Whiteaker, P., Marks, M. J., Collins, A. C., and Lester, H. A. (2004) *Science* **306**(5698), 1029-1032
3. Salminen, O., Drapeau, J. A., McIntosh, J. M., Collins, A. C., Marks, M. J., and Grady, S. R. (2007) *Mol Pharmacol* **71**(6), 1563-1571
4. Nashmi, R., Xiao, C., Deshpande, P., McKinney, S., Grady, S. R., Whiteaker, P., Huang, Q., McClure-Begley, T., Lindstrom, J. M., Labarca, C., Collins, A. C., Marks, M. J., and Lester, H. A. (2007) *J Neurosci* **27**(31), 8202-8218
5. Grady, S. R., Meinerz, N. M., Cao, J., Reynolds, A. M., Picciotto, M. R., Changeux, J. P., McIntosh, J. M., Marks, M. J., and Collins, A. C. (2001) *J Neurochem* **76**(1), 258-268
6. Wooltorton, J. R., Pidoplichko, V. I., Broide, R. S., and Dani, J. A. (2003) *J Neurosci* **23**(8), 3176-3185
7. Pfaffl, M. W. (2001) *Nucleic Acids Res* **29**(9), e45
8. Marks, M. J., Whiteaker, P., Calcaterra, J., Stitzel, J. A., Bullock, A. E., Grady, S. R., Picciotto, M. R., Changeux, J. P., and Collins, A. C. (1999) *J Pharmacol Exp Ther* **289**(2), 1090-1103
9. Marks, M. J., Smith, K. W., and Collins, A. C. (1998) *J Pharmacol Exp Ther* **285**(1), 377-386
10. Drenan, R. M., Nashmi, R., Imoukhuede, P., Just, H., McKinney, S., and Lester, H. A. (2008) *Mol Pharmacol* **73**(1), 27-41
11. Nashmi, R., Dickinson, M. E., McKinney, S., Jareb, M., Labarca, C., Fraser, S. E., and Lester, H. A. (2003) *J Neurosci* **23**(37), 11554-11567